Cape Peninsula University of Technology

Plasma assisted surface treatment of solution deposited CuO:NiO mixed oxides thin film for nonenzymatic glucose detection

by

MAGHMOOD PALMER

A thesis submitted in fulfilment of the requirements for the degree

Master of Engineering: Chemical Engineering

in the Faculty of Engineering and Built Environment

at the Cape Peninsula University of Technology

Supervisor: Dr M. R. Chowdhury (CPUT)

Co-supervisor: Dr J. Chamier (UCT)

and Dr M. Masikini (CPUT)

Bellville

November 2020

DECLARATION

I, Maghmood Palmer, declare that the contents of this dissertation/thesis represent my own unaided work, and that the dissertation/thesis has not previously been submitted for academic examination towards any qualification. Furthermore, it represents my own opinions and not necessarily those of the Cape Peninsula University of Technology.

Signed:  Date: 15 March 2021

ABSTRACT

The amount of people with diabetes mellitus is rapidly increasing with approximately 4.6 million South African sufferers in 2019. Self-management of the illness which includes daily blood glucose concentration tests is costly, stressful, and painful. The most used method for detecting glucose concentration involves an enzymatic sensor. Non-enzymatic sensors, which use metals to directly oxidise glucose, have the potential to replace expensive and complicated enzymatic sensors. Numerous studies have shown that metals, alloys and bimetallic, metal oxides and composites, and carbon-based compounds can be used as catalytic materials for glucose oxidation. Literature suggests that Cu, which is found in natural abundance, has good catalytic properties and stability, and is relatively inexpensive. Furthermore, copper oxide has superior electrocatalytic properties compared to pristine copper. The multivalent states of copper oxide enhance recovery of the electrocatalyst of the electrode surface. However, compared to other metal oxides such as NiO_x and Co_xO_x, copper oxide has a lower conductivity, decreased electroactivity, and limited surface area. Electrocatalytic properties are more tuneable in multi-element nanostructures in comparison to pristine nanostructure. Therefore, the electroactivity of copper oxide is improved by the addition of nickel oxide. Plasma assisted nitrogen doping is used to improve the exposed surface area by etching the surface of the electrode and induces partial conversion of copper (II) oxide into copper (I) oxide. This would be favourable for copper oxide due to the nature of multivalent states which enhances recovery of the electrocatalyst, enhances lifespan of the sensor and introduces a different element into the multielement structure.

To synthesise an electrode, nanostructures are fabricated through various techniques and cast onto a conductive substrate with a binder. Adhesion of the nanostructures to the conductive substrate presents a challenge and the binder used then reduces the electrical conductivity of the electrode. Direct growth of nanostructures onto the conductive substrate can be achieved through hydrothermal techniques or plasma sputtering. Challenges involved in these methods include controlling film thickness and homogeneity and high capital costs. Previously, a low-cost solution deposition-based technique had been used to deposit Co_3O_4 thin films. However, the biggest drawback was controlling the phase and morphology of the deposited film. The interest in this work is therefore to deposit (a) CuO:NiO thin films and (b) induce phase transformation of CuO to Cu_2O by plasma assisted nitrogen doping. It was rationally designed to utilise the mixed oxidation sate of CuO/Cu_2O together with the NiO doping for enhanced electrochemical activity towards glucose oxidation. It will be shown that the as-developed plasma-assisted nitrogen doped mixed oxide (N-CuO/Cu_2O:NiO) thin film has excellent glucose sensing abilities with very high selectivity and an ultrafast response time.

The N-CuO/Cu_2O:NiO sensor was synthesised by making a precursor solution of copper oleate and nickel nitrate. The precursor was then spin coated onto the conductive substrate followed by calcination resulting in mixed oxides of CuO:NiO. Thereafter, the electrodes underwent plasma assisted nitrogen doping. Physical characterisation was performed on the developed electrodes using XRD, XPS, SEM, EDS, and Hall Effect measurements. Electrochemical characterisation was used to compare the glucose sensing abilities of the developed sensors with a pristine CuO sensor.

The pristine host structure of the developed sensor consisted of CuO. Furthermore, NiO nanostructures were present within the host structure of CuO. The SEM results showed that NiO was present in the form of cube-like structures bonded with the CuO. Nitrogen was doped into the electrode though plasma assisted nitrogen doping and induced phase conversion of CuO to Cu_2O. Electrochemical glucose testing showed that the as-developed sensor (labelled as N-CuO/Cu_2O:NiO) showed an ultra-fast response time of 2.5 s with high sensitivity (1131 $\mu A/mM.cm^2$). The linear range of the sensor was calculated to be up to 2.74 mM of glucose and excellent selectivity towards glucose at an applied potential of +0.67 V vs Ag/AgCl in 0.1 M NaOH electrolyte solution. The limit of detection was 20 µM for the N-CuO/Cu_2O:NiO sensor. The N-CuO/Cu_2O:NiO have smaller Tafel slope compared to pristine CuO and CuO:NiO mixed oxides. Enhanced electrochemical performance of the N-CuO/Cu_2O:NiO originates from the improved electronic properties of the thin film.

LIST OF PUBLICATIONS

INYANG, A., KIBAMBO, G., PALMER, M., CUMMINGS, F., MASIKINI, M., SUNDAY, C. & CHOWDHURY, M. 2020. One step copper oxide (CuO) thin film deposition for non-enzymatic electrochemical glucose detection. *Thin Solid Films,* 709**,** 138244

PALMER, M., MASIKINI, M., JIANG, L.-W., WANG, J.-J., CUMMINGS, F., CHAMIER, J., INYANG, O. & CHOWDHURY, M. 2020. Enhanced electrochemical glucose sensing performance of CuO: NiO mixed oxides thin film by plasma assisted nitrogen doping. *Journal of Alloys and Compounds***,** 156900

PALMER, M., MASIKINI, M., JIANG, L.-W., WANG, J.-J., CUMMINGS, F. & CHOWDHURY, M. 2020. Dataset of N-doped CuO: NiO mixed oxide thin film sensor for glucose oxidation. *Data in brief,* 33**,** 106408

Presented at:

2nd Seminar on Nanotechnology
Nanotech@CPUT2019
16 August 2019
Senate Hall, Bellville Campus

ACKNOWLEDGEMENTS

Praise and Thanks to God for giving me strength, knowledge and understanding, and all the countless blessings

This research project was undertaken within the Chemical Engineering Department at the Cape Peninsula University of Technology between January 2018 and January 2020.

I want to express my deepest gratitude to the following people for contributing towards the completion of this thesis:

My Supervisor, Dr Mahabubur Chowdhury, for his excellent supervision, guidance, motivation, and technical expertise. I could not have completed this without you sir. The past 4 years were thrilling, informative and an absolute pleasure to learn from.

My co-supervisors Dr Chamier and Dr Masikini for all the superior assistance and guidance throughout my master's career. And a special mention to Dr cummings for your excellent aid and guidance too.

The technical and administrative staff in the Chemical Engineering Department Mrs Small and Mrs Alberts for all the "behind the scenes" assistance. Me and all other student of CPUT could not graduate without you.

All my aunts and uncles for your love and support for more than 25 years. I owe all of you so much.

My sister and her husband for always being there in any form necessary.

My mom for her unconditional love and support. Words cannot describe my gratitude for you mom. Thank you for everything.

And to my dad and all other deceased, may you all be granted a high place in paradise and may we meet on day.

TABLE OF CONTENTS

LIST OF FIGURES

LIST OF TABLES

LIST OF SYMBOLS

GO_x	Glucose oxidase enzyme
FAD	Flavin adenine dinucleotide
M_{ox}	Mediator in oxidation form
M_{red}	Mediator in reduction form
OH_{ads}	Adsorbed hydroxyls
σ	Standard deviation of chronoamperometric study of blank solution
m	Sensitivity (μA/mM.cm^2)
R_{ct}	Charge transfer resistance (Ω)
W	Warburg impedance (Ω)
R_{sol}	Solution resistance(Ω)
M-	Metal bonded to an element
χ^2	Correlation coefficient
I	Current (A)
X_{conc}	Concentration (mM) of glucose injected

LIST OF ABBREVIATIONS

IDF	International Diabetes Federation
XRD	X-ray diffraction
XPS	X-ray photoelectron spectroscopy
SEM	Scanning electron microscopy
EDS	Energy dispersive x-ray spectroscopy
CV	Cyclic voltammetry
EIS	Electrochemical impedance spectroscopy
RNA	Ribonucleic acid
IHOAM	Incipient hydrous oxide adatom mediator
ITO	Indium tin oxide
FTO	Fluorine doped tin oxide
GCE	Glassy carbon electrode
CPE	Carbon paste electrode
BDD	Boron doped diamond
CNT	Carbon nanotubes
LOD	Limit of detection
CPE	Constant phase element
SEI	Solid-electrolyte interface
AA	Ascorbic acid
UA	Uric acid
MEISP	Multiple EIS parameterization software
RSD	Relative standard deviation

CHAPTER 1: INTRODUCTION

1.1. Background

The cells in our body require energy to function, develop and reproduce (Carrà, 2018, Xiao et al., 2019). This energy is sourced from metabolic processes, which breakdown carbohydrates into energy and other by-products (Cosnier et al., 2014, Scognamiglio, 2013). Glucose is the most predominant carbohydrate used to source energy in human beings. In the human body, glucose is transported by blood and controlled by insulin (Scognamiglio, 2013). Cosnier et al. (2014) suggested that each gram of glucose has the potential to provide 16 kW of energy. Diabetes Mellitus is described as a metabolic disease affecting the body's ability to secrete or use insulin effectively (Association, 2010, Roglic, 2016). Persons afflicted with the disease are required to monitor and manage the disease (Xiao et al., 2019) which can be stressful and costly. The World Health Organisation reported that 422 million people were suffering from diabetes in 2014 (Roglic, 2016). Research conducted by the American Diabetes Association showed that $327 million were used in 2017 for diagnosed management. The International Diabetes Federation (IDF) suggests that of the 501 million people in Africa, aged between 20-79 years, 19 million are suffering from diabetes which contributed to 366 200 deaths and resulted in $10 billion of health expenditure for the year 2019 (Williams et al., 2019). These statistics can be observed in Figure 1-1 and shows that South Africa is rated as the top country in the African region for diabetes sufferers with an estimated value of 4.6 million people (Williams et al., 2019).

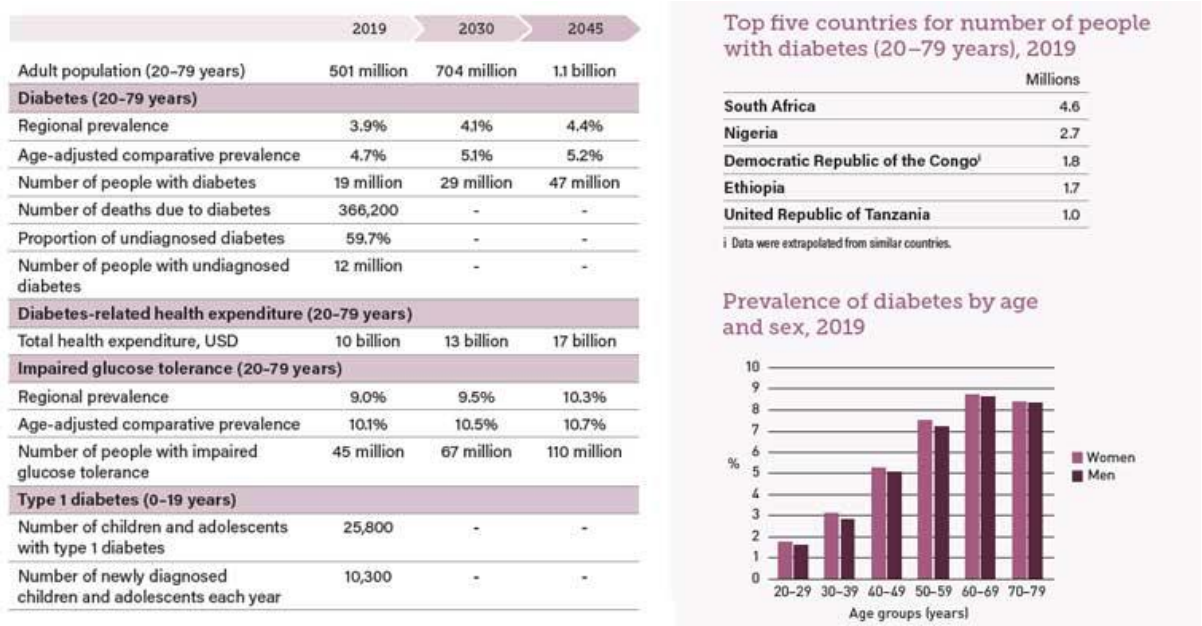

	2019	2030	2045
Adult population (20–79 years)	501 million	704 million	1.1 billion
Diabetes (20–79 years)			
Regional prevalence	3.9%	4.1%	4.4%
Age-adjusted comparative prevalence	4.7%	5.1%	5.2%
Number of people with diabetes	19 million	29 million	47 million
Number of deaths due to diabetes	366,200	-	-
Proportion of undiagnosed diabetes	59.7%	-	-
Number of people with undiagnosed diabetes	12 million	-	-
Diabetes-related health expenditure (20–79 years)			
Total health expenditure, USD	10 billion	13 billion	17 billion
Impaired glucose tolerance (20–79 years)			
Regional prevalence	9.0%	9.5%	10.3%
Age-adjusted comparative prevalence	10.1%	10.5%	10.7%
Number of people with impaired glucose tolerance	45 million	67 million	110 million
Type 1 diabetes (0–19 years)			
Number of children and adolescents with type 1 diabetes	25,800	-	-
Number of newly diagnosed children and adolescents each year	10,300	-	-

Figure 1-1 Diabetes statistics estimated by the International Diabetes Federation (Williams et al., 2019).

Currently, enzymatic glucose sensors are used to monitor blood glucose levels, providing information necessary to determine the dosage of insulin required, if dietary changes are required or adverse medication is necessary (Zhang et al., 2015). Enzymatic sensors use proteins to detect glucose concentrations (Rauf et al., 2016). These sensors make use of the finger prick technique (Du et al., 2016, Zhang et al., 2015), consisting of a finger prick to release blood, placing the blood on the enzymatic strip which can be measured by a sensing device (Scognamiglio, 2013). The perpetual advancement of technology has provided infrastructure able to produce the enzymatic strips effectively at incredible speeds using printing devices (Du et al., 2016). However, these rapidly produced protein-based sensors are vulnerable to proteases, which degrade and digest proteins (Xiao et al., 2019). Furthermore, numerous environmental conditions tend to shorten the life span of the enzymatic biosensor (Rauf et al., 2016, Xiao et al., 2019). Moreover, enzymatic sensors require extensive purification procedures. Hence, there is a need to develop new types of sensors.

1.2. Non-enzymatic glucose detection

The disadvantages of enzymatic sensors have been addressed by developing non-enzymatic sensors with the ability to electrochemically react directly with glucose (Xiao et al., 2019). Xiao et al. (2019) state that the catalytic material plays a key role in glucose oxidation performance. Choosing the right material for non-enzymatic glucose sensing is therefore, of extreme importance. Noble metals such as Pt and Au exhibit good electro catalytic properties during glucose oxidation owing to good electro-activity. However, noble metals more expensive, with lower selectivity, susceptible to poisoning by intermediates (Al-Omair et al., 2017, Guo et al., 2019) and operate at higher potentials (Si et al., 2013). Alloys possess increased optical, electronic and catalytic qualities, when compared to the standalone material, due to the various combinations of materials which is able to complement one another (Tee et al., 2017). However, these properties are highly dependent on material structure, mixing ratios and mixing patterns (Tee et al., 2017).

1.2.1. Transitional metal oxides

Transition metal oxides such as NiO_x, FeOOH, MnO_2, RuO_2, CuO_x, ZnO and Co_3O_4 (Al-Omair et al., 2017), have shown increased application potential. These metal oxides are relatively low in costs with superior glucose sensing ability as not prone to poisoning of the catalytic surface during operation (Wu et al., 2019, Guo et al., 2019). These metal oxides would oxidise glucose at a constant potential creating a simplified process for detection (Tee et al., 2017). Cu and Ni possess good catalytic properties, are found in natural abundance, have good stability and are relatively inexpensive (Tee et al., 2017, Xiao et al., 2019). Studies conducted

by Espro et al. (2014) showed that the oxide form of copper has superior electrocatalytic properties compared to the pristine copper. Copper oxide is also a sought material due to the multivalent states which improve recovery of electrocatalyst (Xiao et al., 2019). Cao et al (2014) state that copper oxide has superior electroactivity compared to nickel oxide. However, copper oxide still suffers poor electrocatalytic activity, low conductivity (Guo et al., 2019) and has limited active surface area compared to other metal oxides such as Co_xO_x and NiO_x (Ko et al., 2013). Literature suggest that multi-element or complex architectures should increase the electrocatalytic properties of metal oxides (Xiao et al., 2019, Wu et al., 2019). The combination of copper oxide and nickel oxide shows favourable electrocatalytic properties (Cao et al., 2011).

1.2.2. Multiple oxidation state of CuO_x

Redox activation of the electrode material plays an important role in enhancing sensitivity of electrode materials for non-enzymatic glucose sensing. Lu et al. (2014) demonstrated that presence of multiple oxidation states in a CuO/Cu_2O composite material improved the electrochemical performance of the material compared to its pristine counterpart (Lu et al., 2014). In an experiment conducted by Masudy-Panah et al. (2015), nitrogen doping of CuO thin film at low temperature showed partial conversion of CuO to Cu_2O. In addition, this incorporation of nitrogen atoms significantly reduces the resistivity of the thin film (Masudy-Panah et al., 2015). Previously, NiO, a *P*-type semiconductor has been utilised as a dopant to enhance the electrochemical properties of CuO microfibres (Cao et al., 2011). Therefore, it is only rational, to design a CuO/Cu_2O:NiO composite material and evaluate the developed material for non-enzymatic glucose detection.

1.2.3. Fabrication methods

Traditionally, developing an electrode for sensing applications involves a two-step process. Firstly, the nanomaterials are prepared via various synthesis routes, such as hydrothermal, solvothermal, and solgel etc. (Wang et al., 2008, Shen and Xia, 2014) which require extensive purification procedures and time consuming operations. These methods are not optimal due to high capital and operational costs (Aditha et al., 2016). Finally, the prepared nanostructured materials are drop casted on a conductive substrate with a binder. The presence of the binder introduces contact resistance which ultimately can reduce electrical conductivity of the materials (Chowdhury et al., 2017b). Moreover, the materials suffer low adhesion onto the substrate. Direct growth of nanostructured materials via the hydrothermal technique has been conducted (Zhuang et al., 2008). However, controlling the film thickness and film homogeneity proved challenging. Techniques such as plasma sputtering and atomic layer deposition can

deposit an uniform controlled film on a substrate (Masudy-Panah et al., 2015). The use of ultrahigh vacuum, however, makes these processes capital intensive. Solution deposition techniques which can be used to develop low-cost electrode with controlled film thickness, is needed. In previous work, a solution-based technique was used to deposit Co_3O_4 thin films (Chowdhury et al., 2017a, Gota et al., 2017, Chowdhury et al., 2017b).

One of the biggest drawbacks of the developed method is the lack of phase and morphology control of the deposited film (Chowdhury et al., 2017a, Gota et al., 2017). Hence, the interest in this work is to deposit (a) CuO:NiO thin films and (b) induce phase transformation of CuO to Cu_2O within the deposited CuO:NiO thin film by plasma assisted nitrogen doping. It was rationally designed to utilise the mixed oxidation sate of CuO/Cu_2O together with the NiO doping for enhanced electrochemical activity towards glucose oxidation. It will be shown that the as-developed plasma-assisted nitrogen doped mixed oxide (N-CuO/Cu_2O:NiO) thin film owns excellent glucose sensing abilities with very high selectivity and ultrafast response time. Physical and electrochemical characterisation techniques will be used and discussed to probe the origin of the enhanced electrochemical activity in the following sections.

1.3. Research problem

Diabetes Mellitus is a growing disease which has devastating effects on the wellbeing of those afflicted by it. These persons are required to permanently monitor their blood glucose concentration which is extremely costly. The current method for detection of blood glucose concentrations is achieved using enzymatic glucose detection strips. Broad-based research has been conducted to replace the current strip with non-enzymatic materials. There is a wide variety of materials, such as noble metals, metal oxides or metal composites, with the potential to replace the proteins within the enzymatic strip. However, there are numerous disadvantages for the non-enzymatic glucose detection materials such as high operational costs and time-consuming procedures to produce highly selective and sensitive materials, relatively cost-effective materials such as CuO_x and NiO suffers from poor electroactivity and limited active surface area.

1.4. Research topic

Modifications of non-enzymatic glucose detectors is abundant due to the availability of many catalytic materials and various processes for the fabrication of the catalytic materials. The electrocatalytic properties of the metal oxide (non-enzymatic) sensor can be improved by the introduction of multi-element species (Xiao et al., 2019, Wu et al., 2019), namely CuO_x and NiO. Plasma assisted nitrogen doping can induce phase transformation of CuO into Cu_2O (Lu

et al., 2014). Lu and company continued by stating that the multiple oxidation state in CuO/Cu_2O had improved the electrochemical performance. The introduction of nitrogen atoms reduced the resistivity of the sensor which related to improved electrochemical performance (Masudy-Panah et al., 2015). Finally, the solution deposition methods were simple and produced low cost electrodes (Chowdhury et al., 2017a, Gota et al., 2017). Therefore, in this work, a plasma-assisted nitrogen doped mixed oxide (N-CuO/Cu_2O:NiO) sensor is developed for the detection of glucose.

1.5. Research questions

i. What are the effects of introducing NiO into the complex structure on the electrocatalytic performance of the developed sensor?
ii. How does plasma-assisted nitrogen doping affect the morphology of the metal oxide used for glucose detection?

1.6. Aims and Objectives

The aim of this research was to develop a plasma-assisted nitrogen doped mixed oxide (N-CuO/Cu_2O:NiO) thin film sensor with enhanced glucose detection ability with reference to a broader linear range, higher sensitivity, and a low detection limit. This was achieved by carrying out the following objectives:

i. Synthesis of Mixed oxide (CuO and NiO) with various ratios to determine the most favourable towards glucose oxidation,
ii. Nitrogen doping of the mixed oxide (CuO:NiO) thin film sensor using a plasma-assisted doping method,
iii. Evaluation of the electrochemical properties of the developed sensor,
iv. Conducting physical characterisation of the developed sensor and their application in glucose detection.

1.7. Delineation

This study will not include the testing of human samples.

Physical characterisations include x-ray diffraction (XRD), x-ray photoelectron spectroscopy (XPS), scanning electron microscopy (SEM), energy dispersive x-ray spectroscopy (EDS), Hall effect measurements and all other methods are delineated.

Evaluation of electrochemical properties includes cyclic voltammetry (CV), chronoamperometric response, Tafel slope measurements and electrochemical impedance spectroscopy (EIS) with all other methods being delineated.

1.8. Thesis outline

Chapter 1 provides information regarding the background of the thesis including the objectives for the study, research questions and the significance of the thesis.

Chapter 2 details an in-depth discussion of the literature study with relation to the topic being studied.

Chapter 3 provides details of the experimental procedures, equipment required, and apparatus used to conduct all necessary experiments.

Chapter 4 a detailed discussion of the results acquired during experimentation.

Chapter 5 gives a conclusion with respect to the result obtained including recommendations.

CHAPTER 2: LITERATURE REVIEW

Nanotechnology is an evolving science and being widely researched for advanced properties and applications. Nanotechnology can be used to develop materials able to catalytically react with compounds and thus can be used as a sensor. A sensor is a device that has the ability to detect an analyte in solution (Toghill and Compton, 2010). Thus, a biosensor detects analytes from human serums which can be in the form of glucose in physiological samples (Hsu et al., 2012). However, glucose biosensors can also be used in monitoring processes within the bio-industrial fields, quality control of process engineering and fuel cells (Si et al., 2013) This section of the report outlines key aspects in diabetes monitoring by use of non-enzymatic biosensor.

2.1. Glucose Monitoring

All cells require energy to develop, reproduce and function (Carrà, 2018, Xiao et al., 2019). The main source of energy in human cells is carbohydrates, which consists of various forms of sucrose, transported by blood within the body and controlled by insulin (Scognamiglio, 2013). Due to various physio-pathological conditions an average human being's glucose level can range between 4-7 mM (Chowdhury et al., 2017a). Abnormal glucose levels may negatively impact the health and wellbeing of the human (Kim and Shim, 2013). Long term patients may suffer from severe complications in the retina and circulatory systems and is the leading cause of mortality in human health (Scognamiglio, 2013, Kim and Shim, 2013). People who have diabetes mellitus (abnormal blood glucose concentrations), are required to monitor, and manage the disease effectively (Xiao et al., 2019, Zhu et al., 2020). Monitoring the disease can be extremely costly, due to the fact that the enzymatic strip used for glucose detection can only be used once (Kim and Shim, 2013, Tee et al., 2017), and can be stressful as a result of lancing the finger at the tip (Feldman et al., 2000, Cash and Clark, 2010), as illustrated in Figure 2-1. The rapid increase in numbers of those afflicted with diabetes has resulted in large investment opportunities for advancement in management of the disease.

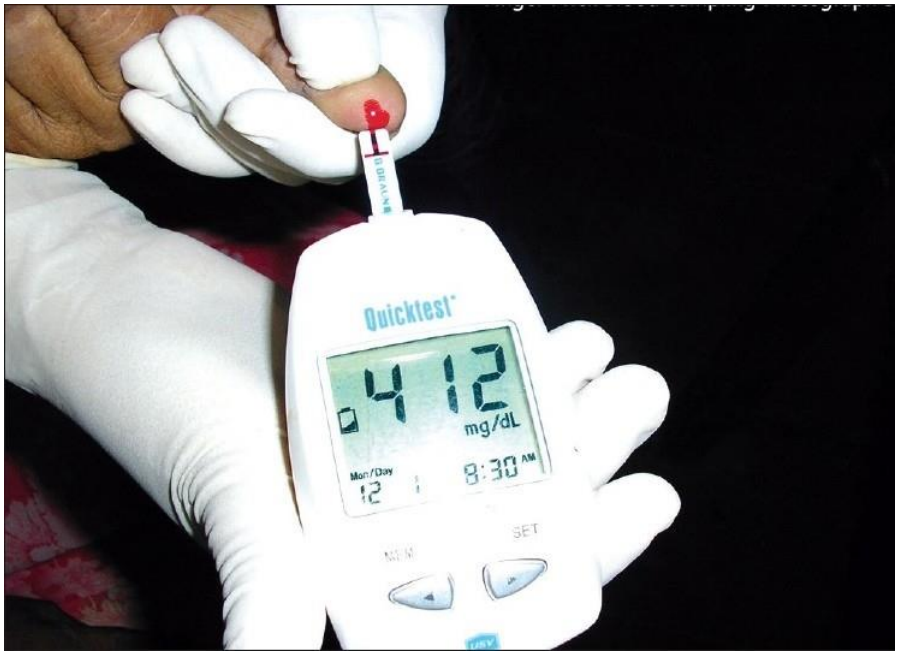

Figure 2-1 Finger-prick glucose detection

(Chopra and Kumar, 2011).

2.2. Enzymatic glucose detection

For the device to be commercialised, the biosensor should be accurate, relatively quick, highly sensitive and reproducible (Ding et al., 2010, Toghill and Compton, 2010). There are two distinct methods of detecting glucose from bodily fluids; enzymatic (uses proteins to facilitate fructose oxidation) and non-enzymatic (uses metal alloys to facilitate fructose oxidation). Many of the more recent enzymatic biosensors are manufactured using various proteins and a few made of RNA molecules (Rauf et al., 2016). Firstly, these proteins are vulnerable to proteases which degrade and digest the proteins (Xiao et al., 2019). Furthermore, various environmental conditions tend to degrade the protein over time which creates a definite shelf life for the product (Xiao et al., 2019, Rauf et al., 2016). Other common disadvantages of enzymatic biosensors include extensive purification procedures, multi-step immobilization procedure requirements, thermal and chemical instability, relatively large production costs and a time-consuming production process (Rauf et al., 2016, Wang et al., 2013). There are various generations of enzymatic biosensors. The first three generations would be described below.

2.2.1. First generation enzymatic glucose biosensor

Enzymatic glucose detection has both great advantages and critical disadvantages (Toghill and Compton, 2010). The first generation of enzymatic sensors is highly oxygen dependant; plays an empirical role in the catalytic reaction and is the determining variable for glucose

detection (Zhu et al., 2016, Tee et al., 2017). The oxidation of glucose is catalysed with glucose oxidase (GO_x) and is observed by the following chemical reaction (Zhu et al., 2016):

$$\text{Glucose} + O_2 \xrightarrow{GO_x} \text{gluconic acid} + H_2O_2 \quad (2.1)$$

The amperometric application, creation of electrode and analysis thereof, of the biosensor was successful (Toghill and Compton, 2010). The high oxygen dependency of the device makes it more difficult to be accurate without negatively affecting the practicality and usage thereof especially in oxygen deficient environments (Zhu et al., 2016, Rauf et al., 2016). Similarly, electro-active species may interfere with the first-generation enzymatic biosensor results (Rauf et al., 2016, Toghill and Compton, 2010). These critical flaws paved the way forward for further studies and modifications.

2.2.2. Second generation enzymatic glucose biosensor

The second generation is able to nullify the oxygen dependency by introducing a mediator and improves its ability to neglect interference by electro-active substances present in bodily fluids (Toghill and Compton, 2010, Tee et al., 2017). Mediators such as ferrocene, ferricyanide and transitional metal complexes, are synthetically created to facilitate electron transfer, thus diminishing oxygen dependency which results in a more sophisticated electrode (Zhu et al., 2016, Toghill and Compton, 2010). The mechanism describing the oxidation of glucose is described in the following reactions (Zhu et al., 2016):

$$\text{Glucose} + GO_x(FAD) \rightarrow \text{gluconic acid} + GO_x(FADH_2) \quad (2.2)$$

$$GO_x(FADH_2) + 2M_{ox} + 2e^- \rightarrow GO_x(FAD) + 2M_{red} + 2H^+ \quad (2.3)$$

$$2M_{red} \rightarrow 2M_{ox} + 2e^- \quad (2.4)$$

M_{ox} and M_{red} represent the mediator in oxidation and reduction forms, and FAD is flavin adenine dinucleotide (Zhu et al., 2016).

The second generation had the potential to overcome limitations of first-generation sensors such as the oxygen dependency and the high susceptibility to interference, but has distinct operable constraints in temperature, humidity, and pH (Toghill and Compton, 2010, Park et al., 2004, Zhu et al., 2016). Mediators have common attributes contributing to effective glucose analysis which include low molecular weights, functionality at lower redox potentials, greater stability, reduced formation of by-products and reduced reversibility due to low solubility (Toghill and Compton, 2010). However, the redox matrix is seen to compete with the mediators creating an ineffective environment for electron transfer (Park et al., 2004).

2.2.3. Third generation enzymatic glucose biosensor

The third generation of enzymatic sensors aimed to eliminate the need of a mediator through direct electron transfer between the enzyme and electrode (Wang et al., 2013, Zhu et al., 2016). The electrode materials consisted of conductive organic salts and other conducting organic substance to facilitate direct electron transfer (Wang et al., 2013). This form of enzymatic sensor requires the enzyme to be immobilized onto the electrode (Zhu et al., 2016). Zhu et al. (2016) described the mechanism for glucose oxidation with the following reactions:

$$\text{Glucose} + GO_x(FAD) \rightarrow \text{gluconic acid} + GO_x(FADH_2) \quad (2.5)$$

$$GO_x(FADH_2) + 2e^- \rightarrow GO_x(FAD) + 2H^+ \quad (2.6)$$

Long chain polymers with high flexibility created an electron relay to successfully modify the glucose oxidase employment onto the electrode surface (Wang et al., 2013). This generation of enzymatic sensors still suffered from limitations in enzyme activity due to temperature and humidity (Zhu et al., 2016). The linear operational range of this generation sensor was smaller when compared to the first two generations (Tee et al., 2017). Therefore, further development of the glucose sensor was still required.

2.3. Non-enzymatic glucose biosensor

Non-enzymatic sensors would create a fourth generation of glucose sensors to address the flaws of the previous generations (Wang et al., 2013, Toghill and Compton, 2010). The aim of the non-enzymatic glucose sensor is to oxidise glucose in solution directly (Toghill and Compton, 2010). The non-enzymatic electrocatalysts can be found in numerous forms such as metals, alloys and bimetallic, materials of a carbon-based nature, metal oxides, and metal-metal oxide composites (Wang et al., 2013, Rauf et al., 2016).

2.3.1. Nanomaterials and nanotechnology

Constructing the biosensor from nanomaterials poses various benefits (Si et al., 2013, Cash and Clark, 2010). Components are more easily interchangeable, have the ability to be miniaturised and can be used during microfluidic integration (Scognamiglio, 2013). Glucose monitoring is a key focus in literature as it occupies approximately 85% of the biosensor market (Si et al., 2013). Monitoring of glucose concentrations can be achieved by electrochemical analysis between the biosensor and the analyte (Luo et al., 2006). Luo et al. (2006) continued by suggesting that the high conductivity of metal nanomaterials would ensure ideal conditions for the electron transfer during the electrochemical reactions.

Nanotechnology involves the study of material properties with extremely small proportions, the dimensions range between 1 and 100 nm (Cash and Clark, 2010). To put this in perspective, the sheet of paper this report is typed on is approximately 100 µm thick (Mousavi et al., 2009). According to Scognamiglio (2013), specific physiochemical processes become enhanced at this scale. These enhanced physiochemical processes include superior plasticity, improved reactivity and activity, quicker electron and ion exchange (Scognamiglio, 2013). It was also observed that nanoscale materials have distinct differences in thermal and optical properties when compared with bulk materials (Cash and Clark, 2010). Superior qualities, summarised in Figure 2-2, allow the nanomaterials to be used in many disciplines and applications (Scognamiglio, 2013).

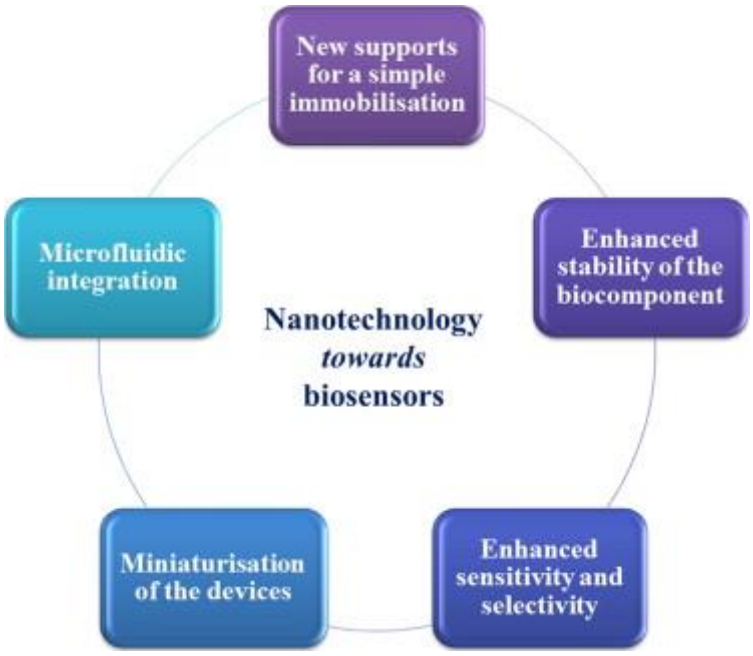

Figure 2-2 Advantages of nanotechnology for use in biosensors (Scognamiglio, 2013).

2.3.2. Theory of electrocatalysis of non-enzymatic materials

The most common forms of non-enzymatic sensors are metals in various forms which are all dependent on a transitional metal centre, excluding carbon based non-enzymatic sensors (Wang et al., 2013, Toghill and Compton, 2010). The adsorption on and change of the analyte on the electrode surface under a potential current is known as electrocatalysis. The electrocatalytic process presumably involves the d-electrons and d-orbitals of the metal nanomaterial allowing for the formation of a suitable bond with the adsorbate (Pletcher, 1984). The bond between adsorbate and metal is required to from and break during the catalytic process and is dependent on the Gibbs energy of adsorption (Toghill and Compton, 2010). Furthermore, Toghill and Compton (2010) suggested that the strength of the bond should not

limit the adsorption capabilities or hinder the desorption of the analyte. The bond with the analyte can be altered through a change in oxidation state of the metal improving the metal-adsorbate interactions. Pletcher (1984) suggested that the catalytic process involves the abstraction of hydrogen and the simultaneous adsorption of the organic species as observed in Figure 2-3 below.

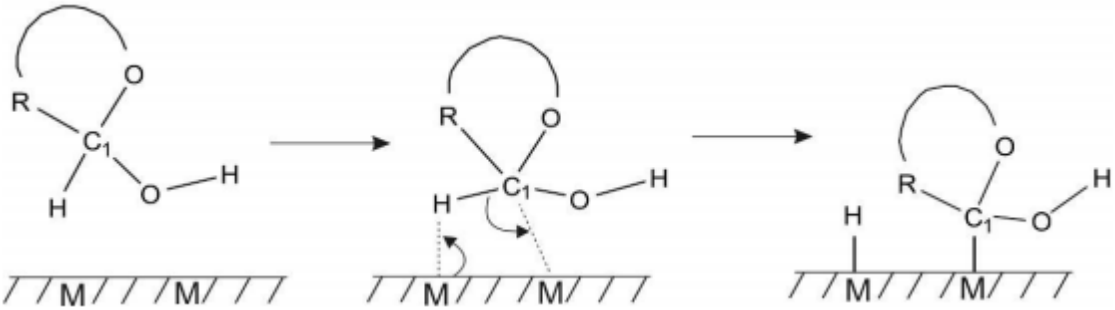

Figure 2-3 Adsorption theory between analyte and metal nanomaterial

(Toghill and Compton, 2010).

The active transition metal core across the electrode only considers the process of adsorption onto the surface, but does not consider the hydroxyl radicals' oxidative role (Toghill and Compton, 2010, Wang et al., 2013). The electrooxidation of glucose occurs with the formation of adsorbed hydroxyls (OH_{ads}) (Lin et al., 2018, Zhu et al., 2018, Yi et al., 2015, Cheng et al., 2019). During the pre-monolayer oxidation step the surface metal atoms forms a hydrous oxide layer of reactive OH_{ads} which mediates oxidation and inhibits reduction of the electrode reactions (Wang et al., 2013, Toghill and Compton, 2010). This process is defined as the incipient hydrous oxide adatom mediator (IHOAM) model (Burke, 1994). The surface of the electrode is more reactive, as they lack lattice stabilization energy because of lower lattice co-ordination values relative to bulk crystal structure. The surface layer therefore, undergoes pre-monolayer oxidation at lower potentials (Toghill and Compton, 2010). Toghill and Compton (2010) continue by affirming the importance of the active OH_{ads} layer due to the rapid formation of the layer and mediates oxidation of the adsorbed compounds at relatively lower potentials illustrated in Figure 2-4. The platinum group metals as well as gold follow the IHOAM model for enhanced catalysis (Toghill and Compton, 2010). However, metals such as nickel and copper use the hydroxyl group to create a change in oxidation state for the electrocatalysis.

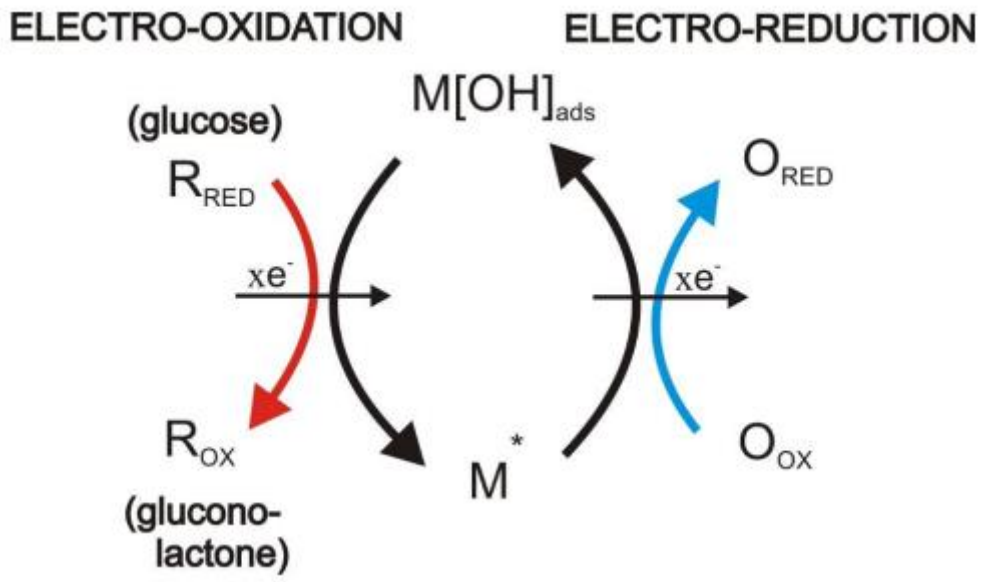

Figure 2-4 Illustration of the reactive metal being used in the IHOAM model (Toghill and Compton, 2010).

2.4. Nanomaterials used in non-enzymatic glucose sensors

Non-enzymatic electrodes has potentially created a fourth generation of glucose sensors which has the ability to directly oxidise glucose in the sample (Toghill and Compton, 2010). The incorporation of nanomaterials allows for increased surface area of the catalytic material, ultimately increasing the reactivity of the material (Tee et al., 2017) and has improved electron transfer between electrode and catalytic material (Cash and Clark, 2010). Non-enzymatic electrocatalyst are present in various forms such as metals, alloys and bimetallic, carbon-based catalysts, and metal-metal oxide nanocomposites (Tee et al., 2017, Wang et al., 2013). In this section of the literature review, a range of nanomaterials used for glucose oxidation are highlighted in Figure 2-5.

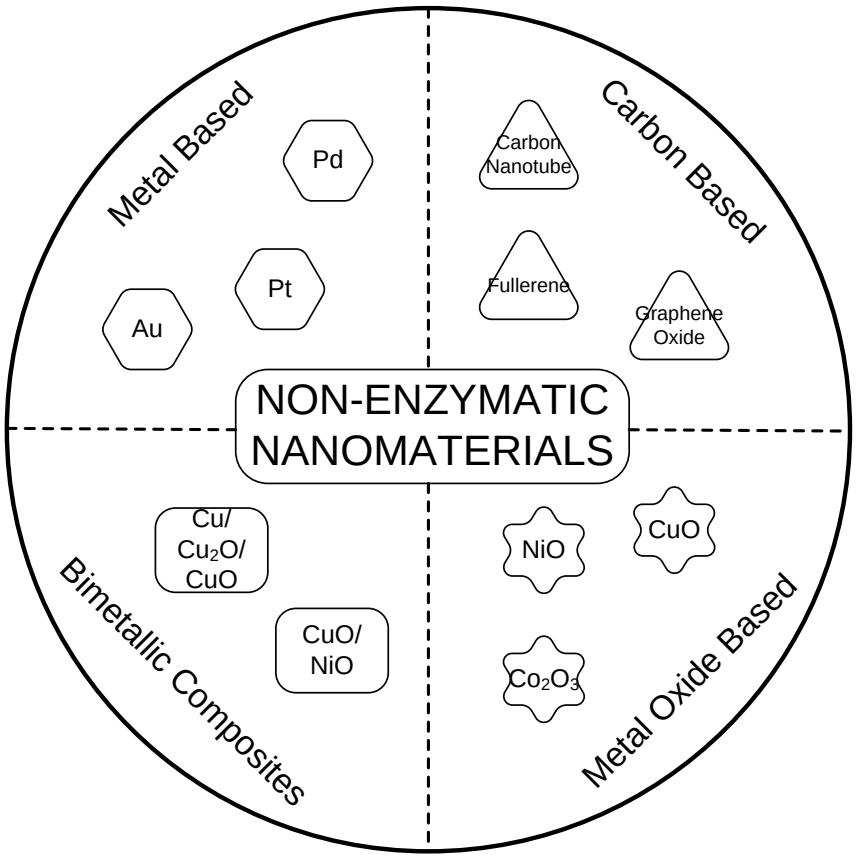

Figure 2-5 Summary of nanomaterials used for non-enzymatic glucose detection

Adapted from (Rauf et al., 2016).

2.4.1. Transitional metals

Transitional metals are effective electrocatalysts due to their ability to transform into multiple oxidations states absorbing other species onto the surface and forming intermediates. A reaction process is created by activating these intermediates (Si et al., 2013). Other advantages of metallic nanomaterials include unique physical, chemical, optical, and electrical properties (Ding et al., 2010, Si et al., 2013). Metallic nanomaterials are mainly used due to their high surface to volume ratio, good electrical conductivity and high electrocatalytic activity (Tee et al., 2017, Si et al., 2013).

2.4.1.1. Gold based non-enzymatic sensors

Non-enzymatic sensors fabricated with gold (Au) nanoparticles have demonstrated the ability to oxidise glucose electrochemically (Si et al., 2013, Rauf et al., 2016). The $AuOH_{ads}$ is involved in the electrooxidation of glucose which is supported by the IHOAM model (Toghill and Compton, 2010):

$$Au + OH^- \rightarrow AuOH_{ads} \quad (2.7)$$

A layer-by-layer deposition of Au nanoparticles onto a thin Au electrode with a sensitivity of 160 μA/mM.cm^2 and a linear range of up to 8 mM for glucose determination has been reported (Kurniawan et al., 2006). A non-enzymatic sensor fabricated through electrodeposition of Au nanoparticles onto an indium tin oxide (ITO) glass electrode achieved a linear range of 0.004-5 mM and a sensitivity of 183.5 μA/mM for glucose detection (Ma et al., 2009). A Au nanowire array electrode was fabricated for the detection of glucose, achieving a linear range up to 10 mM with a sensitivity of 309 μA/mM.cm^2 (Cherevko and Chung, 2009). Recently, a non-enzymatic glucose sensor was fabricated with Au spike-like structures with a linear range of 0.5-30 mM and a sensitivity of 2.4 μA/mM (Hovancová et al., 2020).

2.4.1.2. Platinum based non-enzymatic sensors

Literature suggests that platinum (Pt) shows good electroactivity towards glucose oxidation (Si et al., 2013, Wang et al., 2013). However, due to the flat nature of the Pt electrode, the surface is susceptible to poisoning by physiological substances and environmental conditions, has poor selectivity towards glucose and the flat nature restricts the active surface area (Si et al., 2013, Tee et al., 2017). Therefore, a nano-porous structure of Pt is the most commonly used structure of Pt with improved sensitivity and selectivity compared to the flat electrode (Si et al., 2013). A nano-porous Pt electrode has been fabricated generating a linear range up to 10 mM with a sensitivity of 9.6 μA/mM.cm^2 (Park et al., 2003). Nanotubule arrays of Pt for non-enzymatic glucose detection have been synthesised using electrodeposition with a sensitivity of 0.1 μA/mM.cm^2 and a linear range of 2-14 mM (Yuan et al., 2005). A modified electrode of dendritic Pt was fabricated to electrochemically oxidise glucose without the presence of an enzyme which generated a linear range of 1-20 mM and a sensitivity of 12.1 μA/mM.cm^2 (Shen et al., 2008). A screen-printed glucose sensor comprising of Pt was developed with a linear range up to 13 mm and a sensitivity of 0.167 μA/mM (McCormick and McCrudden, 2020).

2.4.1.3. Nickel based non-enzymatic sensors

The mechanism involved in the electrooxidation of glucose differs from Au and Pt, because it involves the $Ni(OH)_2$/NiOOH redox couple (Si et al., 2013, Tee et al., 2017). The formation of the nickel (Ni) oxyhydroxide is created by the following reaction (Si et al., 2013, Toghill and Compton, 2010):

$$Ni(OH)_2 \rightarrow NiOOH + H^+ + e^- \quad (2.8)$$

A non-enzymatic quantification of glucose was successfully achieved using Ni nanowire arrays generating a sensitivity of 1043 μA/mM.cm^2 for a linear range up to 7 mM (Lu et al., 2009). A glucose sensor of electrospun Ni nanoparticles-loaded carbon nanofibers generated a linear

range up to 2.5 mM with a sensitivity of 420 µA/mM.cm^2 (Liu et al., 2009). Ni nanoparticles implanted on an ITO electrode through the process of ion implantation generated a sensitivity of 577 µA/mM.cm^2 with a linear range of up to 10 mM (Tian et al., 2013). A non-enzymatic sensor consisting of Ni nanoparticles embedded on mesoporous carbon nanorods generated a sensitivity 210.6 µA/mM.cm^2 for a linear range of 0.5-3.03 mM of glucose (Jia et al., 2020). It is clear that Ni has a great sensitivity towards glucose oxidation however, it is highly dependent on the OH^- ions in a basic solution and has a poor selectivity for glucose oxidation (Si et al., 2013, Toghill and Compton, 2010).

2.4.1.4. Copper based non-enzymatic sensors

The electrooxidation of glucose using copper (Cu) is similar to that of Ni, but uses the redox couple of Cu(II) and Cu(III) for the catalytic reaction (Si et al., 2013, Wang et al., 2013). Electrocatalysts comprising of Cu has increased due to its economic viability without compromising sensitivity or selectivity (Wang et al., 2013). A glucose non-enzymatic sensor was made with Cu nanobelts which generated a sensitivity of 79.8 µA/mM.cm^2 for a linear range up to 1.13 mM (Huang et al., 2009). A sensitivity and linear range for an electrode with Cu nanowires, used for glucose oxidation, was 420.3 µA/mM.cm^2 and 2 mM respectively (Zhang et al., 2012a). A novel glucose sensing electrode was fabricated using Cu nanoparticles decorated on nitrogen-doped graphene to achieve a sensitivity of 48.13 µA/mM.cm^2 for a linear range up to 4.5 mM (Jiang et al., 2014). Nitrogen doped graphene was attached to a glassy carbon electrode followed by electrodeposition of Cu nanostructures onto the host structure which generated a linear range of up to 5 mM of glucose and a sensitivity of 1848 µA/mM.cm^2 (Gowthaman et al., 2017).

2.4.1.5. Metal oxides

Metal oxides such as NiO, CuO_x, and CoO_x have shown increased application potential for glucose oxidation (Al-Omair et al., 2017). Fabrication of sensors comprising of metal oxides have become popular due to their ease of fabrication (Rauf et al., 2016). These metal oxides are relatively low in costs with superior glucose sensing ability compared to their metallic counterparts (Espro et al., 2014) and they avoid poisoning of the catalytic surface during operation (Wu et al., 2019, Guo et al., 2019). Metal oxide based sensors are also favoured due to their glucose oxidising ability at a constant potential enabling a simple detection process (Tee et al., 2017).

2.4.1.6. Cobalt oxide based non-enzymatic sensors

The first glucose sensing electrode, using cobalt oxide, was fabricated in 2010 and oxidised glucose using the following chemical reaction (Ding et al., 2010):

$$2CoO_2 + \text{glucose} \rightarrow 2CoOOH + \text{gluconolactone} \quad (2.9)$$

This sensor was fabricated using electrospun fibres of cobaltosic oxide (Co_3O_4) immobilized onto a glass electrode generating a linear range of up to 2.04 mM with a sensitivity of 36.25 μA/mM.cm^2 (Ding et al., 2010). Acicular cobaltous oxide (CoO) nanorods-modified electrode was synthesised with a sensitivity of 571.8 μA/mM.cm^2 and a linear range up to 3.5 mM (Kung et al., 2011). A freestanding electrode of Co_3O_4 nanowires decorated on 3D graphene was fabricated generating a linear range up to 0.08 mM with a sensitivity of 3390 μA/mM.cm^2 for glucose detection (Dong et al., 2012). Zn doped Co_3O_4 film was attached to fluorine doped tin oxide (FTO) glass electrode through a binder-less procedure generated a sensitivity of 193 μA/mM.cm^2 for a linear range of up to 0.62 mM of glucose (Chowdhury et al., 2017a).

2.4.1.7. Nickel oxide based non-enzymatic sensors

Similar to the Ni based non-enzymatic sensor, the nickel oxide (NiO) reaction mechanism uses the redox couple $Ni(OH)_2$/NiOOH (Si et al., 2013). The following reactions best describe the electrooxidation of glucose using NiO (Zhu et al., 2018, Si et al., 2013):

$$NiO + OH^- \rightarrow Ni(OH)_2 \quad (2.10)$$

$$Ni(OH)_2 + OH^- \rightarrow NiOOH + H_2O + e^- \quad (2.11)$$

$$NiOOH + \text{glucose} \rightarrow Ni(OH)_2 + \text{gluconolactone} \quad (2.12)$$

A non-enzymatic glucose sensor with nano NiO modified carbon paste electrode exhibited a sensitivity of 0.04 μA/mM.cm^2 for a linear range up to 0.11 mM of glucose (Mu et al., 2011). Nanocomposite electrode consisting of NiO decorated multiwalled carbon nanotubes on a glassy carbon electrode was synthesised generating a linear range up to 3.6 mM with a sensitivity of 691.3 μA/mM.cm^2 (Yi et al., 2015). A glassy carbon electrode, modified with NiO nanofibers, for the detection of glucose, exhibited a sensitivity of 1100 μA/mM.cm^2 with a linear range up to 0.6 mM of glucose (Zhang et al., 2012b). Nitrogen doped carbon spheres decorated with Ni/NiO nanostructures generated a sensitivity of 87.88 μA/mM.cm^2 for a glucose linear range of up to 2.5 mM (Zhu et al., 2018).

2.4.1.8. Copper oxide based non-enzymatic sensors

Copper oxide (CuO) has become one of the most studied nanomaterials (Si et al., 2013) due to its natural abundant (Tee et al., 2017) and that copper oxide has multivalent states which aid in recovery of the electrocatalyst (Xiao et al., 2019). The following reactions are used to describe the glucose oxidation mechanism for both cuprous oxide (Cu_2O) and cupric oxide (CuO) (Lin et al., 2018):

$$Cu_2O + 2OH^- + H_2O \rightarrow 2Cu(OH)_2 + 2e^- \quad (2.13)$$

$$Cu(OH)_2 + OH^- \rightarrow CuOOH + H_2O + e^- \quad (2.14)$$

$$CuO + OH^- \rightarrow CuOOH + e^- \quad (2.15)$$

$$CuOOH + glucose \rightarrow Cu(OH)_2 + gluconolactone \quad (2.16)$$

A CuO nanowires modified Cu electrode fabricated for enzymeless glucose oxidation exhibited a sensitivity of 490 μA/mM.cm^2 with a linear range up to 2 mM (Zhuang et al., 2008). CuO nanofibers were electrospun and thermally treated to fabricate a sensor with a sensitivity of 431.3 μA/mM.cm^2 with a linear range up to 2.5 mM (Wang et al., 2009). A Cu working electrode was modified with in situ growth of CuO nanowires for the detection of glucose generating a linear range up to 2 mM and a sensitivity of 1800 μA/mM.cm^2 (Espro et al., 2014). Cu/Cu_2O/CuO hollow spheres composite structure prepared using an aerosol furnace achieved a sensitivity of 8726 μA/mM.cm^2 for a linear range up to 30 mM of glucose (Lin et al., 2018).

2.4.2. Bimetallic and alloy composites

The bimetallic materials used for non-enzymatic glucose detection have become the superior form of electrocatalyst as it exhibits favourable electronic properties and excellent catalytic activity compared to the monometallic counterparts (Tee et al., 2017, Wang et al., 2013). As a result of synergetic behaviour between the two elements in a composite structure, the electrooxidation of glucose is increased with reduced interferences and poisoning by other species (Si et al., 2013, Wang et al., 2013). Properties and application of bimetallic materials depend on size, shape and composition of the elements (Tee et al., 2017). Electrocatalyst consisting of bimetallic materials are in the form of alloys, adatoms and metal (oxide)/metal oxide composites (Toghill and Compton, 2010, Si et al., 2013). Their properties may vary according to mixing patterns and thus their interfaces can play a significant role (Tee et al., 2017).

The first alloy used to show the increased catalytic activity towards small organic compounds consisted of platinum (Bagotzky and Vassilyev, 1967). In recent years, the study of bimetallic materials has increased tremendously. A non-enzymatic glucose sensor comprising of copper oxide doped nickel oxide microfibres exhibited a sensitivity of 3165.5 μA/mM.cm^2 for a linear range of 0.51 mM (Cao et al., 2011). A CuO/Cu_2O nanofiber composite electrode used for glucose oxidation resulted in a sensitivity of 830 μA/mM.cm^2 and a linear range of up to 10 mM (Lu et al., 2014). A zinc doped Co_3O_4 enzymeless glucose sensor was fabricated with a linear range of up to 0.62 mM of glucose with a sensitivity of 193 μA/mM.cm^2 (Chowdhury et al., 2017a). Ni doped CuO nanowires were constructed for glucose oxidation and exhibited a linear range of up to 3 mM with a sensitivity of 5610.6 μA/mM.cm^2 (Bai et al., 2017).

2.4.3. Carbon based non-enzymatic sensors

Materials consisting of carbon are the most commonly used substance for the synthesis of electrochemical biosensors as a result of their electronic conductivity and electrochemical inertia (Si et al., 2013). Of the carbon based materials, glassy carbon electrode (GCE), carbon paste electrode (CPE) and boron doped diamond (BDD) are more commonly used as electrodes in industrial processes (Toghill and Compton, 2010, Si et al., 2013). A pristine GCE exhibited electrochemical inactivity and therefore a very small anodic current response to glucose (Vassilyev et al., 1985). CPE is used due to its simplistic and low cost preparation procedure as well as it simple surface regeneration (Si et al., 2013). BDD serves as an ideal electrode for surface modification due to its low capacitive current, inert surface, resistance to fouling and increased potential range (Toghill et al., 2010). In the last decade development of carbon based structures such as fullerene, carbon nanotubes (CNT), carbon nanofibers, graphene and doped diamond-like structures have peaked interest for electrochemical biosensors (Wang et al., 2013, Toghill and Compton, 2010). These developed carbon based materials are used due to their good conductivity, high surface area, ease of functionality and good biocompatibility (Si et al., 2013, Wang et al., 2013). However, these materials are mainly used as supporting structures for glucose oxidation electrode (Si et al., 2013).

CHAPTER 3: RESEARCH METHODOLOGY

This chapter provides detailed information regarding the equipment, materials and experimental procedures used to conduct the experimental processes. Included, is a description of the instrumentation used. A quantitative and qualitative approached was used to conduct the experiments.

The experimental procedures can be divided into three separate sections which include:

i. Fabrication of the thin film electrodes.
ii. Electrochemical evaluation of the synthesised electrodes.
iii. Surface characterisation of the thin film electrodes.

Fabrication and electrochemical evaluation of the electrodes were carried out at Cape Peninsula University of Technology, Bellville Campus, Chemical Engineering and Chemistry Building in the Oil and Gas Lab 1.27.

Plasma assisted nitrogen doping, scanning electron microscope images (SEM), energy dispersive x-ray spectroscopy (EDS) and hall effect measurements were conducted at the physics department of University of Western Cape, Bellvile-7535, South Africa

X-ray diffraction (XRD) and x-ray photoelectron spectroscopy (XPS) experiments were conducted at the State Key Laboratory of Crystal Materials, Shandong University, Jinan, Shandong 250100, P. R. China.

3.1. Study of electrochemistry

Most biosensors currently being studied involve electrochemical transduction, in the forms of amperometry, potentiometry, voltammetry or conductometry (Scognamiglio, 2013, Yoon, 2013). The study of these concepts provides quantifiable data which can be used to determine the effectiveness of the biosensor. Electrochemistry is governed by the basic principle of Ohm's Law, which states that resistance to flow is equivalent to the ratio of potential across the component and the current passing through the said component (Broster et al., 2007).

3.1.1. Conductometry

Changes in electrical conductivity can serve as a function of analyte concentrations. This method is dependent on interaction of the analyte in solution which acts as a conductive polymer to span the gap between two adjacent electrodes (Yoon, 2013). The electrochemical cell would have the ability to operate at fixed potentials, optimizing the observations recorded of the cell (Yoon, 2013).

3.1.2. Potentiometry

The potentiometric sensing techniques are unique due to the analyte inducing chemical potential changes in the system, provided no current is flowing (Yoon, 2013). The circuit remains open and the system is then monitored for changes in potentials which have been hypothesised to be proportional to the logarithm of the concentration of analyte (Yoon, 2013). Furthermore, the system is required to be at equilibrium for both chemical and diffusion processes to achieve a thermodynamically accurate response creating as optimum signal to measure (Yoon, 2013).

3.1.3. Amperometry

Amperometry has two basic design specification types namely single potential amperometry and variable potential amperometry. Both designs are based on the principle of redox reactions with the ability to generate current in the solution (Yoon, 2013). A working electrode is able to complete the circuit allowing a flow of current, which is measurable, to be subjected to Faraday's law as a result of dynamic reactions (Bard and Faulkner, 2001, Yoon, 2013).

Various concentration of the analyte is added successively at a given time interval while operating at a fixed potential to evaluate the sensor performance, known as chronoamperometric study (Chowdhury et al., 2017a, Ding et al., 2010). A typical step response would be observed as the analytes is injected into the solution (Yang et al., 2017a).

Using this data, a dosage response curve is achieved by plotting the analyte concentration versus the peak oxidation current recorded using the chronoamperometric study. The linear regression ($R^2 > 0.99$) of the dosage response curve is used to quantify the sensitivity, linear range, and limit of detection (Chowdhury et al., 2017a, Ding et al., 2010). The limit of detection can be calculated using the following formula (Chowdhury et al., 2017b):

$$LOD = \frac{3\sigma}{m} \quad (3.1)$$

σ represents the standard deviation recorded during the chronoamperometric study of the blank solution, i.e. before glucose is added, and m represents the slope of the linear range, i.e. sensitivity (Chowdhury et al., 2017b).

3.1.4. Voltammetry

Similarly, voltammetry also has variable potential amperometry which measures changes in current based on variable potentials (Yoon, 2013). Voltammetry can be used to optimized experimental conditions used for the detection of the analyte using the developed sensor (Yi et al., 2015). It can be used to determine the most effective sensor for the detection of the analyte as a result of a greater peak current observed during tests (Chowdhury et al., 2017b). Voltammetry records the potential at which the analyte is oxidised which would be used during the fixed potential amperometry (Chowdhury et al., 2017b, Yi et al., 2015). The Tafel slope measurements are conducted by converting the voltammetry current plots into log functions (Gloaguen et al., 1994). The Tafel slope quantifies the catalytic mechanism during electrochemical oxidation and thus a smaller slope would result in a faster reaction (Xu et al., 2017).

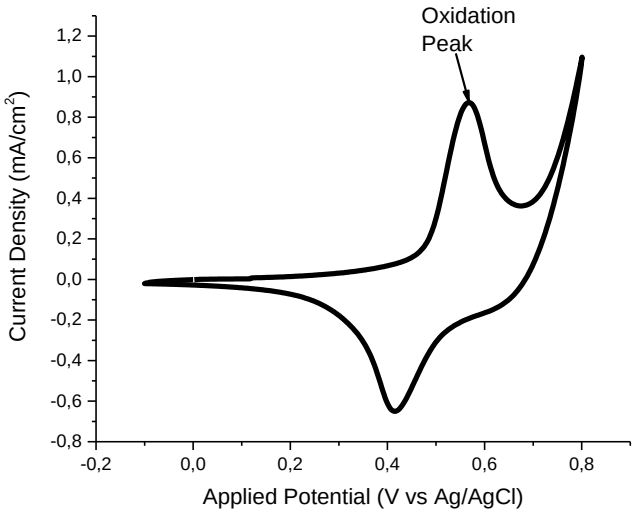

Figure 3-1 Identifying the oxidation peak of the CV diagram

Adapted from (Chowdhury et al., 2017b).

3.1.5. Electrochemical impedance spectroscopy

Electrochemical impedance spectroscopy was used in this study to investigate the charge transfer resistance of the electrodes (R_{ct}). The Nyquist plots recorded exhibit two depressed semi-circles and a straight line in the low-frequency region as observed in Figure 3-2. The semi-circle represented at higher frequencies region can be assigned to the double layered capacitance of the electrode-electrolyte interaction and the overall charge transfer resistance (MacDonald and Andreas, 2014, Li et al., 2015a), the semi-circle at lower frequencies can be assigned to the faradaic reaction (Fasmin and Srinivasan, 2017), and the linear diffusion can be modelled using a Warburg impedance (W) (Li et al., 2015a).

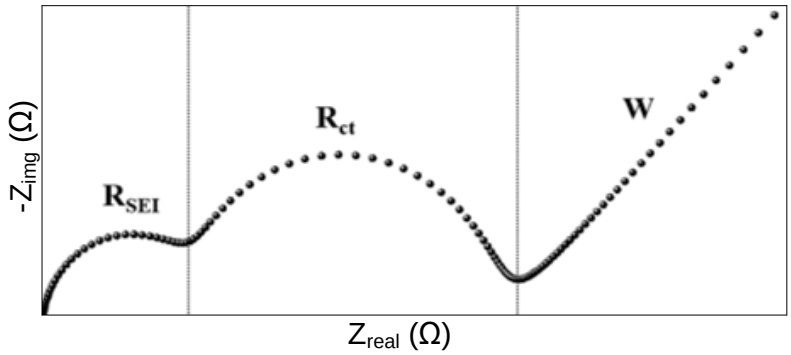

Figure 3-2 Represents the complex plane plot (Nyquist plot)

Adapted from (Choi et al., 2020).

Constant phase elements (CPE) are used instead of a regular capacitor to achieve a more accurate modelling of the EIS data (Choi et al., 2020). An equivalent electrical circuit proposed for fitting the data is shown in *Figure 3-3*. This is an approximation of the complex plane system generated by the EIS experiments (MacDonald and Andreas, 2014, Choi et al., 2020). The circuit at the limit of high frequency quantifies the solution resistance (R_{sol}) representing the flow of electrons through the electrolyte solution (Fasmin and Srinivasan, 2017, MacDonald and Andreas, 2014). The elements represented by R_{SEI} and CPE_{SEI} models the solid electrolyte interface (SEI) diffusion impedance (Li et al., 2015a, MacDonald and Andreas, 2014). The charge transfer resistance (R_{ct}) quantifies the resistance to the flow of ions at the electrode and electrolyte interface (Li et al., 2015a).

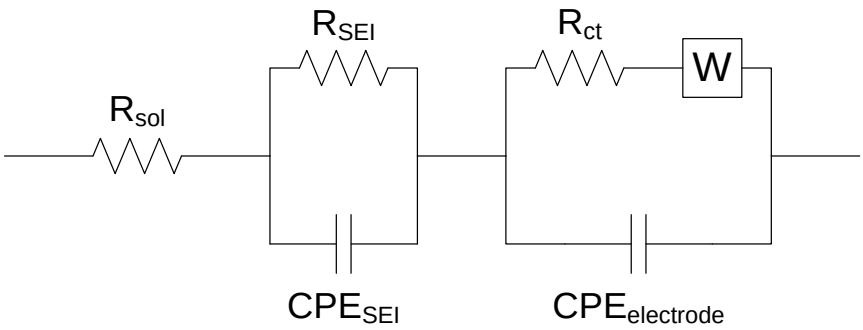

Figure 3-3 Represents the equivalent circuit used to fit the EIS data (MacDonald and Andreas, 2014).

3.1.6. Hall effect measurements

Hall effect measurement is a significant testing technique used for quantifying properties of a conductive material such as carrier concentrations and mobility of the free electrons (Werner, 2017). Other key properties determined by this technique includes resistivity, conductivity and the type of the semi-conductive material (Tyagi et al., 2012, Gessert et al., 2011). An additive to the host can act as 2 distinct types namely *N*-type; where the additive donates an electron to the host lattice generating a negative carrier concentration, and *P*-type semiconductor; where the additive accepts an electron creating a vacancy and results in a positive carrier concentration (Werner, 2017, Tyagi et al., 2012). Literature suggests that higher mobility of the free electron is preferred because it has an inverse relation with the carrier concentration thus producing less optical reflection and absorption (Gessert et al., 2011). The higher mobility also results in superior crystallinity, and reduced scattering centres for charge carriers of the catalytic material (Tyagi et al., 2012).

3.2. Physical characterization of the material

Characterisation of the surface of the electrode is of extreme importance as it quantifies what elements are present on the electrode surface. It also determines structural features, state of the elements and morphology of the surface. The characterisation techniques include X-ray diffraction (XRD), X-ray photoelectron spectroscopy (XPS), scanning electron microscopy (SEM), energy dispersive X-ray spectroscopy (EDS) and hall effect measurements.

3.2.1. X-ray diffraction (XRD)

XRD can be used to determine the nature of the materials as crystalline or amorphous (Vishwakarma and Uthaman, 2020). This non-destructive technique is used to characterize crystalline materials by providing information on structures, phases, preferred crystal

orientations (texture), and other structural parameters (Kohli and Mittal). XRD peaks are achieved through constructive interference of a monochromatic beam of X-rays scattered at specified angles and the peak intensities are determined by the atomic positions within the lattice planes (Kohli and Mittal, Goldstein et al., 2003). Thus, the XRD pattern provides a fingerprint of atomic arrangements of a sample and can be identified using the standard database (JCPDS database) (Vishwakarma and Uthaman, 2020).

3.2.2. X-ray photoelectron spectroscopy (XPS)

XPS is a quantitative technique used for measuring elemental composition of a material analysed through the detection through the binding energies of photoelectrons (Mather, 2009, Baer and Thevuthasan, 2010). This technique is based on a relatively simple process. Electrons within a material absorb photons of a specific energy to emerge from the solid (Engelhard et al., 2017, Baer and Thevuthasan, 2010). The kinetic energy of the electrons emitted from the surface is analysed and provides information on the electronic states of atoms (Engelhard et al., 2017). Small variations in binding energies of the photoelectron lines as well as Auger lines, satellite peaks, and multiple splitting can be used to identify chemical states (Baer and Thevuthasan, 2010).

3.2.3. High resolution surface imaging

High-resolution scanning electron microscopy (SEM) image analysis can determine shape, size distribution, and crystallography of the material, and combined with energy-dispersive X-ray spectroscopy (EDS) can provide more information (Baer and Thevuthasan, 2010). Areas ranging up to 1 mm^3 can be accurately analysed with this combination (Uchic et al., 2007). A high-energy ion beam combined with a fine current can be used over a specific surface area resulting in controlled surface material removal due to sputtering, which can be controlled to 10 – 15 nm per slice (Baer and Thevuthasan, 2010). After each slice, SEM or EDS could be utilized to record information regarding structural, chemical, and surface morphology (Baer and Thevuthasan, 2010).

3.3. Thin film electrode fabrication

3.3.1. Materials

Copper (II) chloride dihydrate ($CuCl_2.2H_2O$), nickel (II) nitrate hexahydrate ($Ni(NO_3)_2.6H_2O$), ethanol, hexane, toluene, sodium oleate ($C_{18}H_{33}NaO_2$) and fluorine doped tin oxide (FTO) glass were purchased from Sigma Aldrich South Africa, deionised water and detergent were

produced in-house by CPUT Bellville. All materials, besides FTO glass, were used without any further purification procedures.

3.3.2. Methodology of mixed oxide thin film electrode

Copper oleate was synthesised by ion exchange reaction between $CuCl_2.2H_2O$ and $C_{18}H_{33}NaO_2$ as reported in previous studies (Park et al., 2004). 20 mmol of $CuCl_2.2H_2O$, 60 mmol of $C_{18}H_{33}NaO_2$, 40 ml of ethanol, 70 ml of hexane and 30 ml of deionised water were measured accurately and placed in a three neck round bottom flask. A condenser, thermometer and a stopper were placed in each neck respectively. The setup was placed onto a heating mantel and a cooling system was connected to the condenser. The mixture was refluxed at 70°C for a total of four hours which allowed for the ion exchange reaction to take place. Thereafter, the mixture was washed three times to remove all by products. The final mixture was poured into a petri dish, covered with parafilm, and placed into a 60°C oven overnight allowing for the excess moisture to be evaporated. This procedure created a wax like substance of copper oleate.

FTO glass slides were cut to size (1.2x4.5cm) and washed extensively in an ultrasonic bath using detergent or degreaser for 10min, followed by an ethanol bath for 10min and finally in water for 10min. The FTO glass slides were dried in a 60°C oven over night following the cleaning procedure. Solution A of 0.09 g copper oleate was sonicated in 0.5 ml of toluene and solution B of 0.01 g $Ni(NO_3)_2.6H_2O$ was dispersed in 0.5 ml of ethanol. The nickel concentration was varied whereby solutions A and B were mixed thoroughly via ultrasonication in volumetric percentage ratios (70:30, 80:20, 90:10 and 95:5). A 50 µL aliquot of the precursor solution was deposited onto the cleaned FTO glass and spin coated in a twostep process to minimise edge/corner beads formation and to produce a uniform layer (Chowdhury et al., 2017b). The FTO glass with precursor was spun at 1000 rpm for 10s followed by 4000 rpm for 50s. Thereafter, the glass electrode was calcined at 350°C for 10min. The deposition, spin coating and calcination were repeated 1 – 6 times (each repetition is described as another layer forming onto the FTO glass slides) to achieve an optimum film thickness for improved electrochemical evaluation.

3.3.3. Plasma assisted nitrogen doping of mixed oxide thin film

To obtain nitrogen doping, the films were plasma irradiated using the CADAR (Cluster Apparatus for Device Application Research) hosted by the Solid-State Physics Group of the University of the Western Cape, Cape Town South Africa. The CADAR system is a custom-built plasma-enhanced chemical vapor deposition, hot-wire chemical vapor deposition and

thermal evaporation system multi-use facility. Of particular interest to this study is the radio-frequency (RF) plasma generating unit of the CADAR system, used for the irradiation of the thin films. The plasma unit employs a COPRA GTE 160 plasma beam source which generates a maximum plasma power output of 600W at a maximum Helmholtz coil current of 3 A and RF frequency of 13.56 MHz.

The plasma is typically ignited by the creation of a pressure pulse, with the N_2 gas fed directly into the excitation cavity of the plasma source. Mass flow controllers (MFC) controls the gas flow to the plasma source. Resonant excitation of the plasma is achieved by applying a weak DC transverse magnetic field, generated by means of a series of built in Helmholtz coils situated inside the plasma source. The strength of the magnetic field is controlled by an auxiliary power supply or so-called COPRA Control Unit (CCU). Figure 3-4 shows a schematic lay-out of the COPRA plasma system of the CADAR Facility.

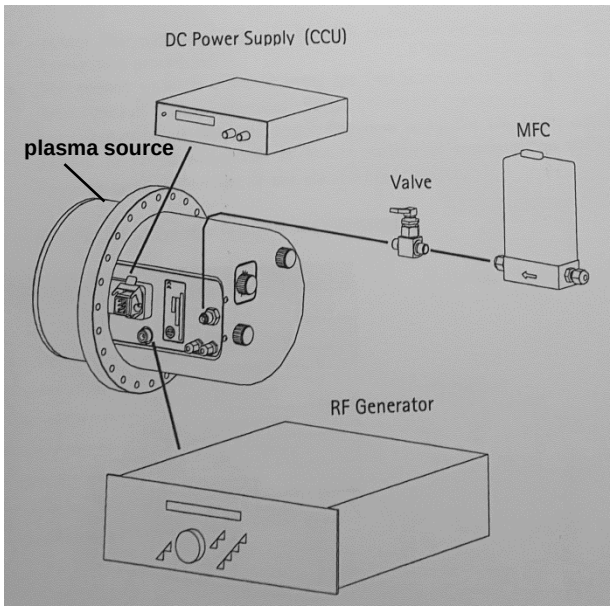

Figure 3-4 COPRA plasma generating unit of the CADAR processing facility, hosted at UWC.

During a typical nitrogen doping experiment, a base and treatment pressure of $1.5x10^{-6}$ and $7x10^{-2}$ mbar, respectively were maintained. Beforehand, the plasma power was optimised in a N_2:Ar gas mixture by establishing a constant gas flow rate of 100:100 sccm. An optimized plasma power of 500 W (and CCU power supply = 5 V; 1.25 A) yielded the most consistent and significant changes. Once set, the Ar flow was reduced to 0 sccm, which resulted in the red glowing N_2 plasma. This point signalled the start of the treatment, which was set at 10 mins for all samples. A summary of the electrode fabrication process is presented in Figure 3-5.

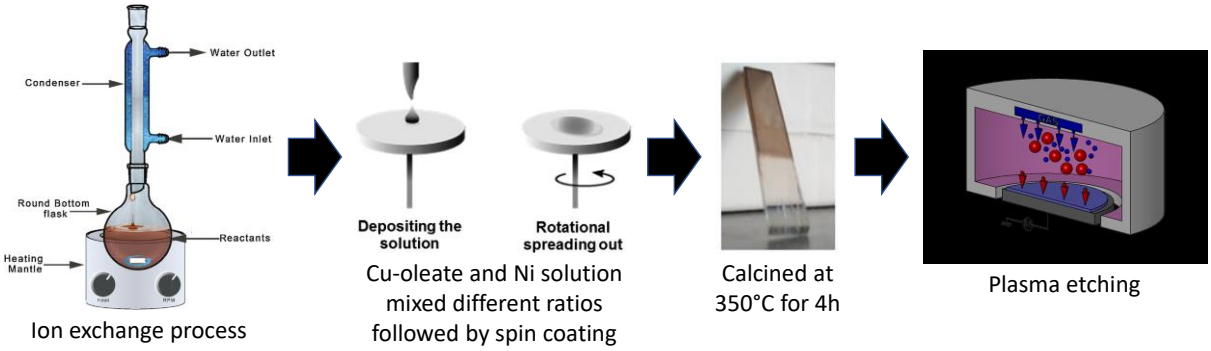

Figure 3-5 Schematic of electrode fabrication process

3.4. Electrochemical evaluation

3.4.1. Materials

Sodium hydroxide (NaOH), d-(+)-glucose, ascorbic acid (AA), uric acid (UA), sucrose, fructose and human serum were purchased from Sigma Aldrich South Africa, and deionised water produced inhouse by CPUT Bellville were used without any further purification procedures.

3.4.2. Methodology of electrochemical evaluations

The electrochemical evaluations were all conducted using an Autolab PGSTAT302N potentiostat (Metrohm, Switzerland). Experiments were performed with a three-electrode setup (seen in Figure 3-6): the as prepared electrodes as working electrodes, an Ag/AgCl reference electrode and a platinum wire counter electrode. A solution of 0.1 M NaOH was used as the electrolyte. The cyclic voltammograms were recorded in the potential range of -0.1 V to 0.8 V vs Ag/AgCl at 25 mV/s in a 0.1 M NaOH solution with various concentrations of glucose. The mixture of glucose in electrolyte was stirred prior to cyclic voltammetry tests.

Constant stirring conditions were applied for the chronoamperometry experiments using an applied bias potential of 0.67 V vs Ag/AgCl. Increasing concentrations of glucose (0.05 – 7.5 mM) was added to the electrolyte solution at 30 sec intervals. The interference tests were conducted using the same chronoamperometric testing procedure. However, glucose (0.2 mM), ascorbic acid (0.02 mM), uric acid (0.02 mM), sucrose (0.02 mM), fructose (0.02 mM) and human serum (0.02 mM) were added at 1 min intervals.

EIS was determined at a bias potential of 0.3 V with 10 mV amplitude as the AC voltage in a frequency range between 1 Hz to 1000 MHz within a 0.1 M NaOH electrolyte solution. The EIS results are presented as Nyquist plots and were fitted using Multiple EIS Parameterization (MEISP) software.

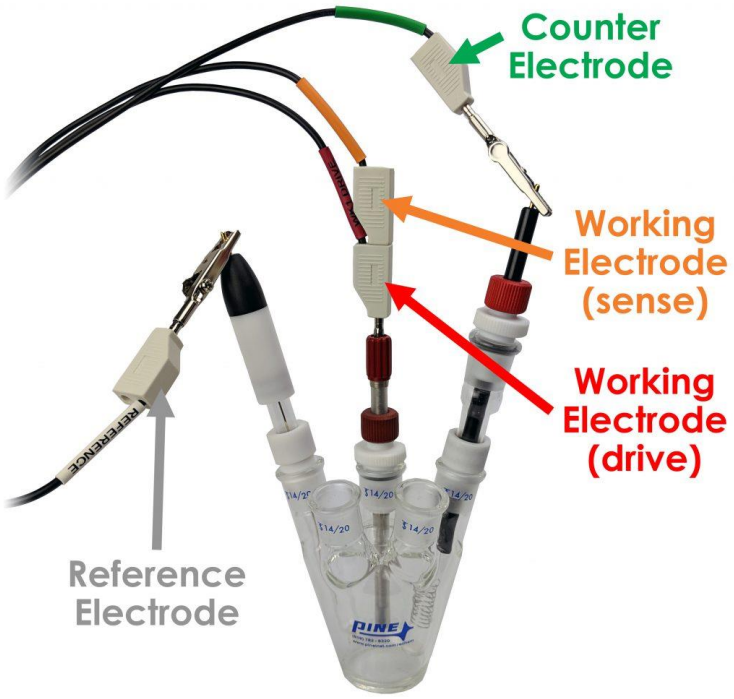

Figure 3-6 Schematic of three electrode setup

(Pine Research, 2019).

3.5. Surface characterisation

3.5.1. Methodology for physical characterisation

The material phase was identified using X-ray diffraction (XRD). The prepared samples were characterized with a Bruker D8 ADVANCE with a Cu Kα radiation source (λ = 0.154178 nm) operated at a tube voltage of 40 kV and a current of 40 mA. The diffraction patterns were collected by step scanning in the 2θ range of 10-70° with an increment of 0.0216°.

X-ray photoelectron spectroscopy (XPS) analysis was performed on a PHI X-tool fully automatic scanning microregion XPS probe (Ulvac-Phi) using monochromatic aluminum as the excitation source. The survey spectra of the electrocatalytic material were recorded with a pass energy of 160 eV and high-resolution spectra with a pass energy of 40 eV.

Zeiss Auriga field emission scanning electron microscope was used to study the morphology of the films produced. All thin films were imaged using an in-lens secondary electron detector with the beam accelerated to an electron high tension of 5 kV.

Energy dispersive x-ray spectroscopy was used to quantify the elemental composition of the films; an Oxford X-max solid-state drift detector was used, with the electrons accelerated to 20 kV.

The electrical transport properties of the films were investigated with Hall Effect measurements using an Ecopia HMS-3000 Hall Effect Measurement System with a 0.55 tesla (T) permanent magnet operated at room temperature. Input currents ranging from 100 to 1000 μA, with 6 measurements on different areas per input current, were applied to reduce the systematic errors and obtain a narrow distribution in mobility, carrier density, resistivity, and dopant concentration.

3.6. Apparatus used for experimental procedures

- Reflux setup: this apparatus would be used to host the ion exchange process between the $CuCl_2.2H_2O$ and $C_{18}H_{33}NaO_2$.

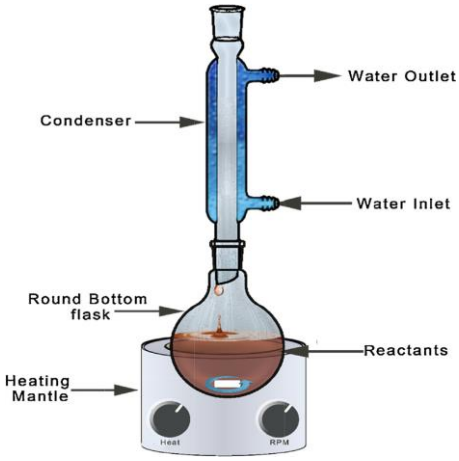

Figure 3-7 Reflux setup

(Aditha et al., 2016).

- Spin coater: used to create a thin film of precursor on the FTO glass electrodes.

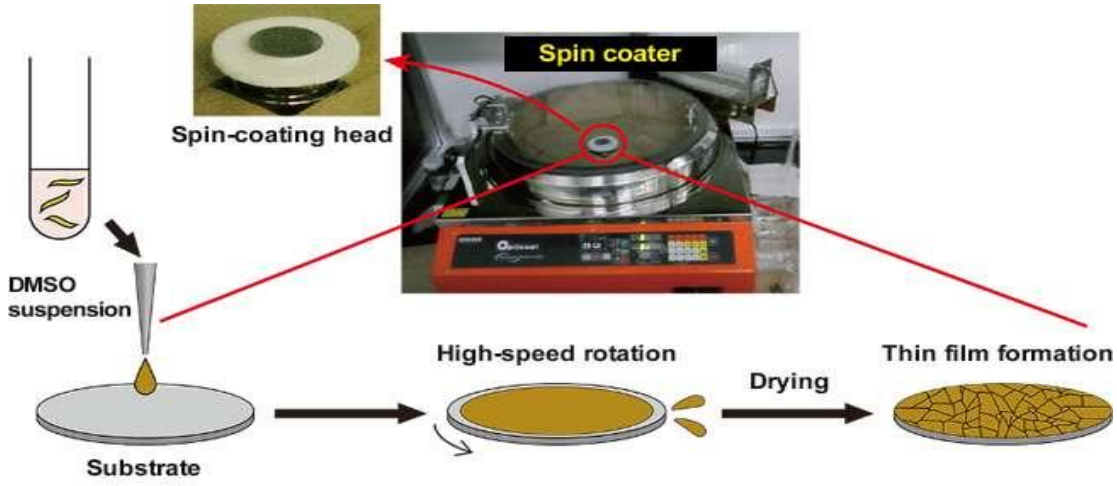

Figure 3-8 Representation of the thin film production using a spin coater

(Phys, 2017).

- Autolab PGSTAT302N potentiostat

Figure 3-9 Potentiostat

(Labmate-online, 2011).

Chapter 4: RESULTS AND DISCUSSION

This chapter aims to show results obtained during the experimental procedures and discusses important findings. The results can be subdivided into two distinct sections namely:

i. Surface characterisation of the synthesised thin film electrodes.
ii. Electrochemical evaluation of the produced thin film electrodes.

4.1. Surface characterisation of the thin film electrode

Characterisation of the surface of the electrode is of extreme importance as it quantifies what elements are present on the electrode surface. It also allows for the determinations of the structural features present and the state of the elements present. The morphology of the surface can also be identified through the various characterisation techniques used. Certain characteristics such as mobility and conductivity can be determined using these techniques. The characterisation techniques include X-ray diffraction (XRD), X-ray photoelectron spectroscopy (XPS), scanning electron microscopy (SEM), energy dispersive X-ray spectroscopy (EDS) and hall effect measurements.

4.1.1. X-ray diffraction (XRD)

X-ray diffraction is a tool that can identify the structural features of various chemical compounds and nanoparticles (Song et al., 2015). The analysis of Figure 4-1a suggests that a base-centred monoclinic structure of CuO was present in the pristine film (Eswar et al., 2018, Manyasree et al., 2017). The diffraction patterns were observed to be at 2θ = around 35.56°; 37.74°; 38.76°; 54.50°; and 61.61° corresponding to (002), (111), (200), (-020), and (-113) respectively, in accordance with the JCPDS Ref. 045-9537 and JCPDS Ref.80-0076 (Eswar et al., 2018). This result confirmed the presence of CuO. The addition of Nitrogen via plasma etching had no clear effect on the diffractogram shown in Figure 4-1b. The diffractogram shows the peaks of CuO in the nitrogen doped CuO film without showing any significant shifts or broadening of XRD peaks of pristine CuO. No Cu_2O peaks were observed. However, it does decrease the intensity of the peaks similar to previously published report (Xu et al., 2017, Muthusankar et al., 2018). In Figure 4-1c the introduction of nickel precursor in the copper oleate precursor during the synthesis decreased the XRD peak intensity of the resulting film. However, Figure 4-1c shows no conclusive Ni or NiO peaks in the diffractogram. The absence of the NiO or Cu_2O characteristic peak may suggest that the quantity of NiO or Cu_2O was below the detection limit of XRD techniques employed. The NiO and Cu_2O may be in an amorphous state thus making it undetectable by XRD. No additional peaks or changes were observed in XRD pattern after plasma treatment of the aforementioned film (data not shown).

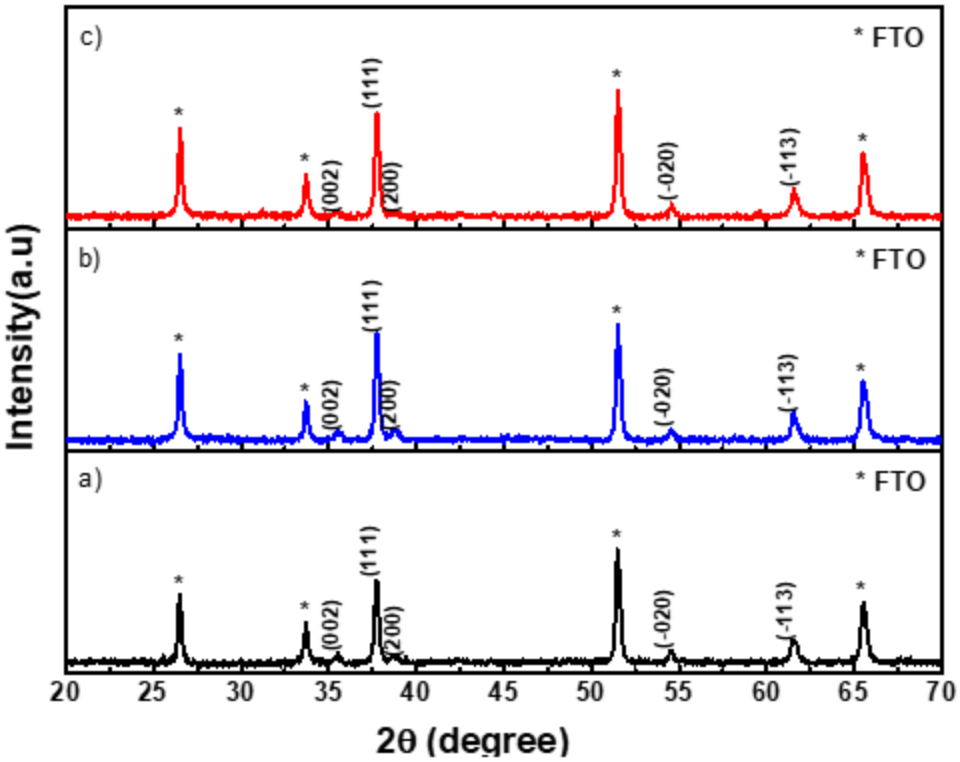

Figure 4-1 XRD diffractogram of the a) pristine CuO film, b) plasma treated CuO film and c) film prepared with nickel precursor

4.1.2. X-ray photoelectron spectroscopy (XPS)

XPS results for the pristine CuO electrode (Figure 4-2) shows a $Cu2p_{3/2}$ peak at 933.3 eV followed by the two satellite peaks at 940.9 and 943.4 eV. Moreover, it also shows a $Cu2p_{1/2}$ peak at 953.3 eV and its satellite peak at 961.8 eV which matches the standard CuO XPS spectrum (Bai et al., 2017, Li et al., 2015b). The oxygen binding energy of peaks 529.3 eV, which represents a common (metal) M-O bond (Cheng et al., 2019, Liu et al., 2016), and 531.0 eV confirms the existence of oxygen in the CuO lattice and hydroxyl absorption which takes place on the electrode surface (Li et al., 2015b, Dar et al., 2008). The O1s peak observed at 531.8 eV suggests that carbon contaminants are present on the electrode material, which indicates a C=O bond (Dhara et al., 2015). This is as a result of the sensor being stored in air. These results confirm the presence of CuO in the pristine electrode and agrees very well with the results obtained from the XRD analysis.

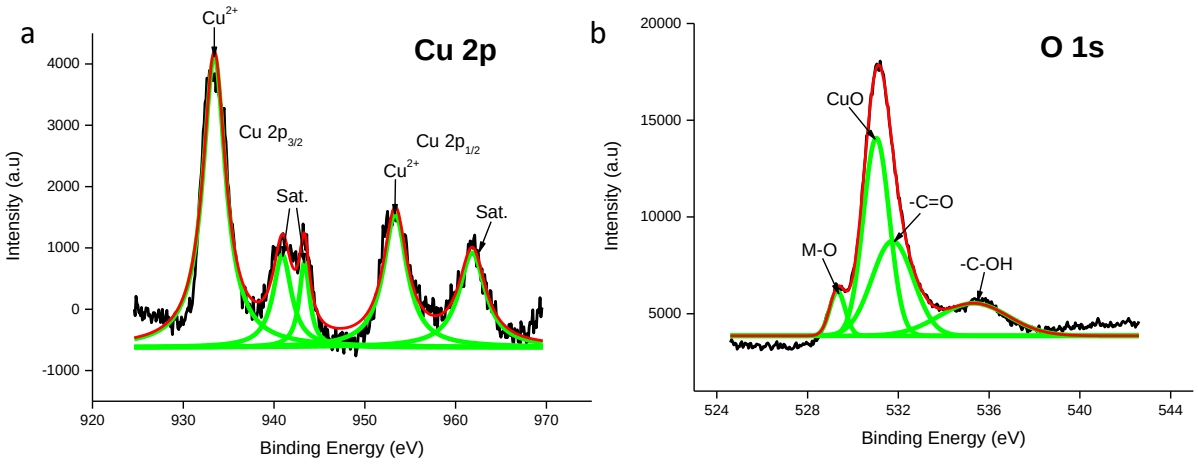

Figure 4-2 XPS data of the CuO electrode highlighting the a) Cu 2p and b) O 1s shells

Introducing nitrogen into the pristine CuO electrode by plasma treatment shows a presence of Cu(I) due to the $Cu2p_{3/2}$ peak observed at 932.5 eV and $Cu2p_{1/2}$ peak at 952.7 eV (Biesinger, 2017, Masudy-Panah et al., 2015). The XPS result in Figure 4-3 also shows a peak at 934.3 eV, indicating the presence of $Cu(OH)_2$ (Biesinger et al., 2010). The N1s spectrogram shows a clear presence of nitrogen within the plasma treated CuO electrode with a peak observed at 397.2 eV. This N1s peak indicated the existence of a M-N species in the form of pyridinic nitrogen (Wagner et al., 2003a, Soto et al., 2004, Zhu et al., 2018). A N1s peak of 398.5 eV hints to the existence of C-N (Wagner et al., 2003a) which may be a result of contamination with common hydrocarbons in the air. Literature suggests that a N1s peak of 403.4 eV creates a nitrite bond of $N\text{-}O_2$ with the host structure (Wagner et al., 2003b, Kabir et al., 2016) and the binding energy of 406.8 eV suggest that other oxidised nitrogen species are present (Matanovic et al., 2016).

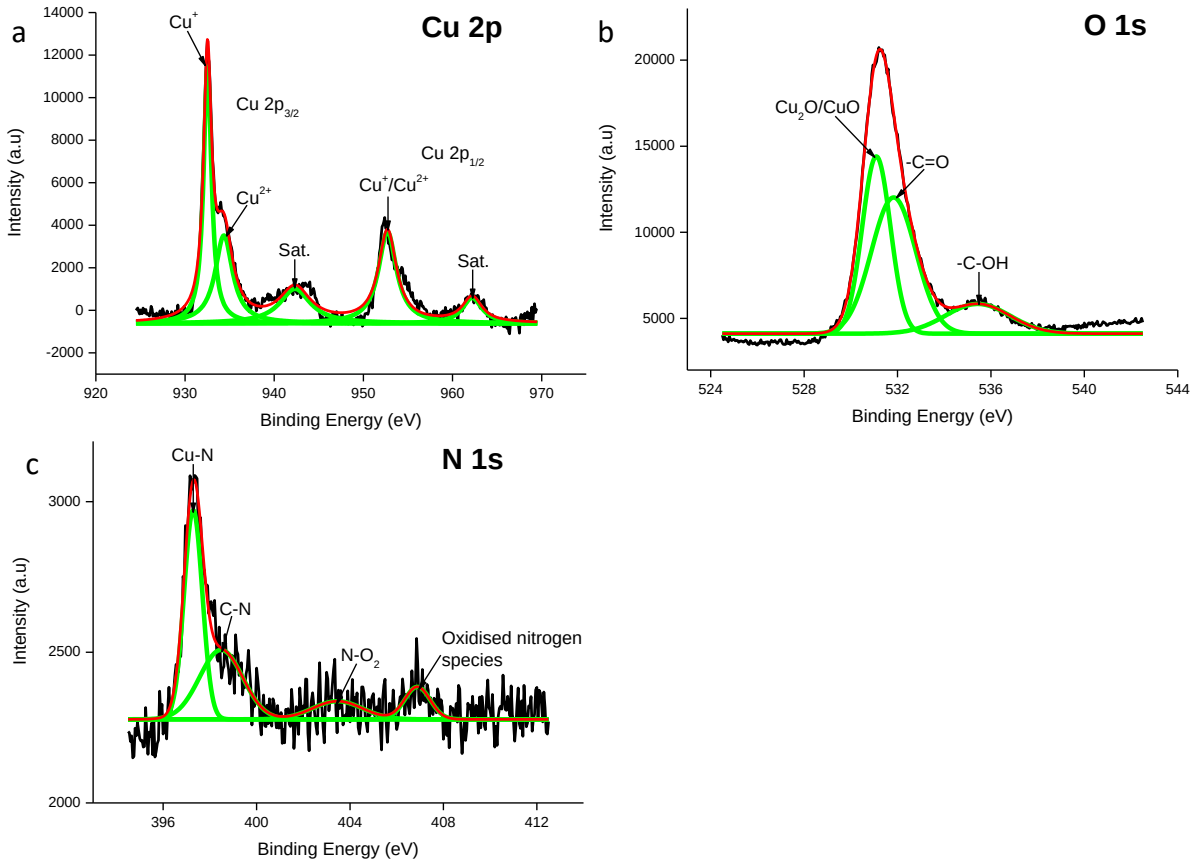

Figure 4-3 XPS data of plasma treated CuO film specifically focussing on the a) Cu 2p, b) O 1s and c) N 1s orbital shells

A Ni $2p_{3/2}$ peak of 855.5 eV was observed (Figure 4-4) for the as prepared electrode corresponding with a satellite peak at 861.2 eV suggesting that the as prepared electrode has NiO within the active material (Zhu et al., 2018, Xiao et al., 2019). Simultaneously, a Ni $2p_{1/2}$ peak at 873.2 eV and a satellite peak at 880.1 eV further confirm the existence of NiO. The slight increase in binding energy of Ni compared to literature suggests that there are interactions with other species (Zheng et al., 2018). The corresponding Cu spectrum also shows the presence of Cu_2O, however, the presence of Ni increases the binding energy suggesting interactions between Cu and Ni in the as prepared electrode. The binding energy of the O1s spectrum at 529.1 eV also confirms the existence of NiO (Zhu et al., 2018, Xiao et al., 2019) and 532.1 eV corresponds to the formation of Cu_2O (Biesinger, 2017, Xiao et al., 2019) within the as prepared electrode. Nitrogen incorporation enhances the electrical conductivity as a result of the availability of p-electrons (Zhu et al., 2018). However, interactions of copper with nitrogen is present due to the lower binding energies of Cu (Zheng et al., 2018). Moreover, the presence of Cu $2p_{3/2}$ peaks of 932.5 and 934.4 eV suggest the presence of $Cu(OH)_2$ together with Cu_2O in the electrode (Guo et al., 2019, Biesinger, 2017). The N1s spectrum suggest that pyrrolic nitrogen is present due to the peak of 399.3 eV, which corresponds to a M-N bond (Zhu et al., 2018). The other peaks are consistent with the N1s

spectrum observed for the plasma treated CuO electrode. It is therefore clear that phase conversion of CuO to Cu_2O occurs during plasma assisted nitrogen doping. Hence the as prepared electrode labelled as N-CuO/Cu_2O:NiO will be discussed from here unless otherwise stated. XPS results of the N-CuO/Cu_2O:NiO after electrochemical evaluations (Figure 4-5) showed no changes in the spectrogram compared to the clean electrode. This highlights the chemical stability of the N-CuO/Cu_2O:NiO electrode.

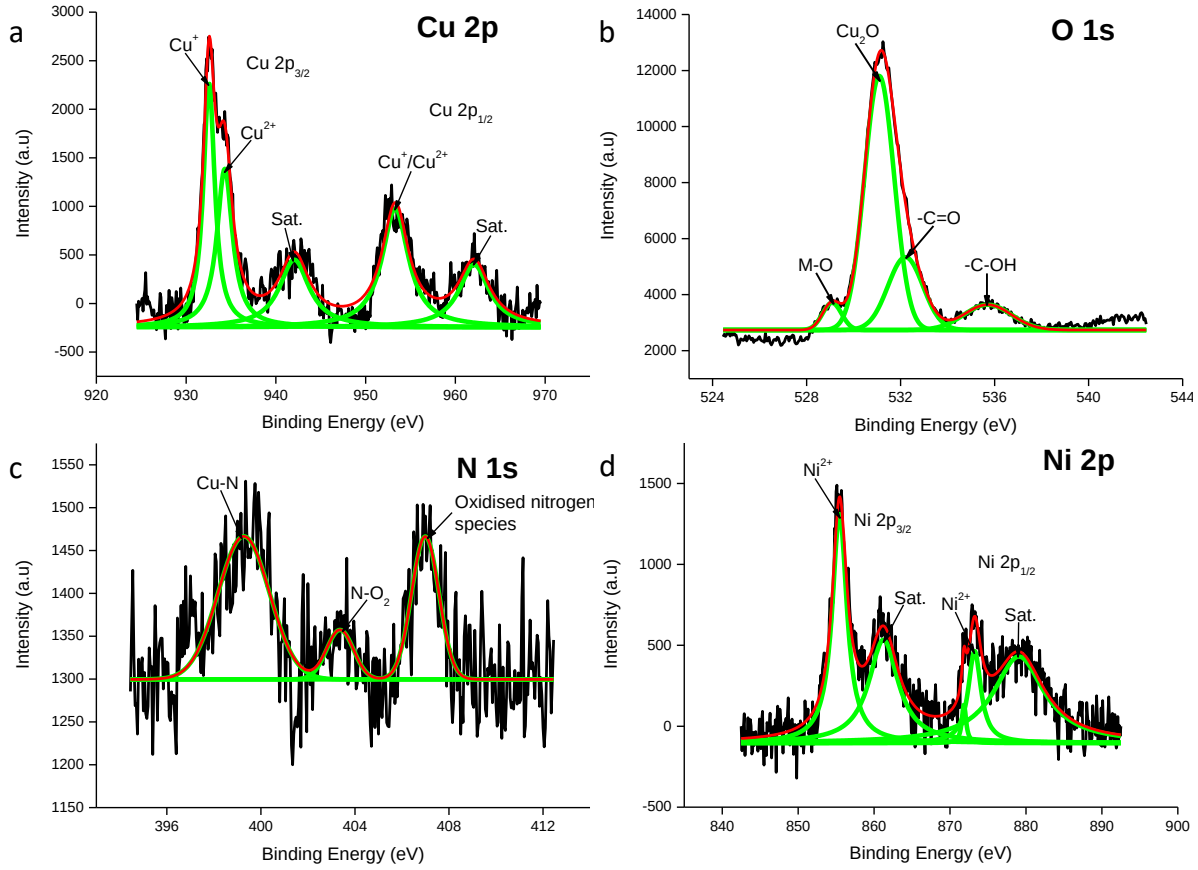

Figure 4-4 XPS spectrogram of the plasma treated CuO:NiO film developed sensor highlighting the peaks present in the a) Cu 2p, b) O 1s, c) N 1s and d) Ni 2p shells

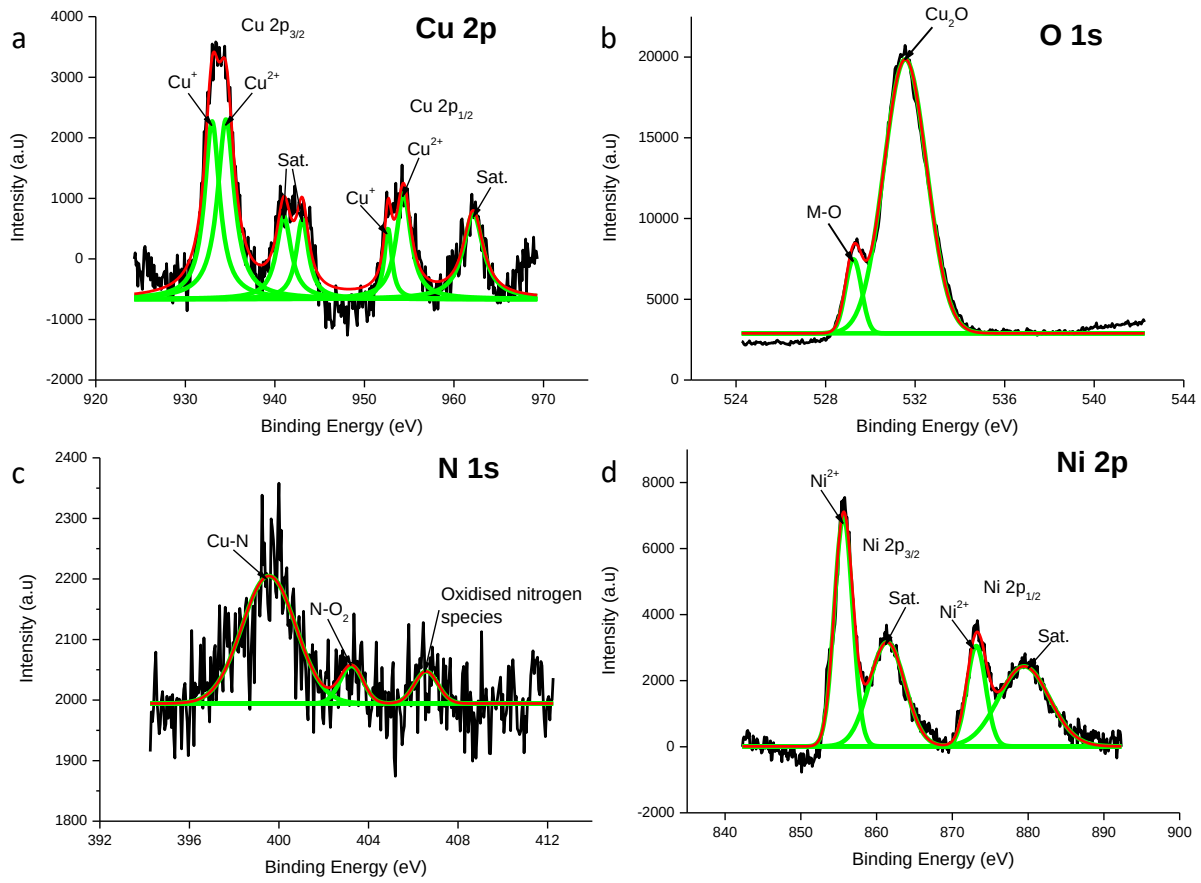

Figure 4-5 XPS data of N-CuO/Cu_2O:NiO after electrochemical tests have been conducted, highlighting active peaks of the a) Cu 2p, b) O 1s, c) N 1s and d) Ni 2p shells

4.1.3. Scanning electron microscopy (SEM) and energy dispersive x-ray spectroscopy (EDS)

Morphology of the thin film electrodes were analysed using scanning electron microscopy (SEM). The SEM images (Figure 4-6a) of the pristine CuO electrode shows a crack free layer with a slight roughness across the surface. Post plasma treatment however, the surface roughness became much smoother and more consistent (Figure 4-6b). This suggests that the introduction of nitrogen via plasma treatment etches the surface roughness of the pristine CuO electrode (Donnelly and Kornblit, 2013). Plasma etching with nitrogen had no other destructive effects on the film morphology. Introducing the nickel precursor into the pristine CuO, as seen in Figure 4-6c, creates cube-like structures of NiO with an average particle size of 200-400 nm forming on top of the base layer of active material. Plasma treated (Figure 4-6**Error! Reference source not found.**d) CuO/NiO electrode shows that the clusters become more pronounced and the average particle size distribution is more centralised at 200-400 nm (Figure 4-7). The presence of Ni and N was also observed from the energy dispersive X-ray spectroscopy, EDX as shown in Figure 4-6e cementing the conclusion obtained from XPS data.

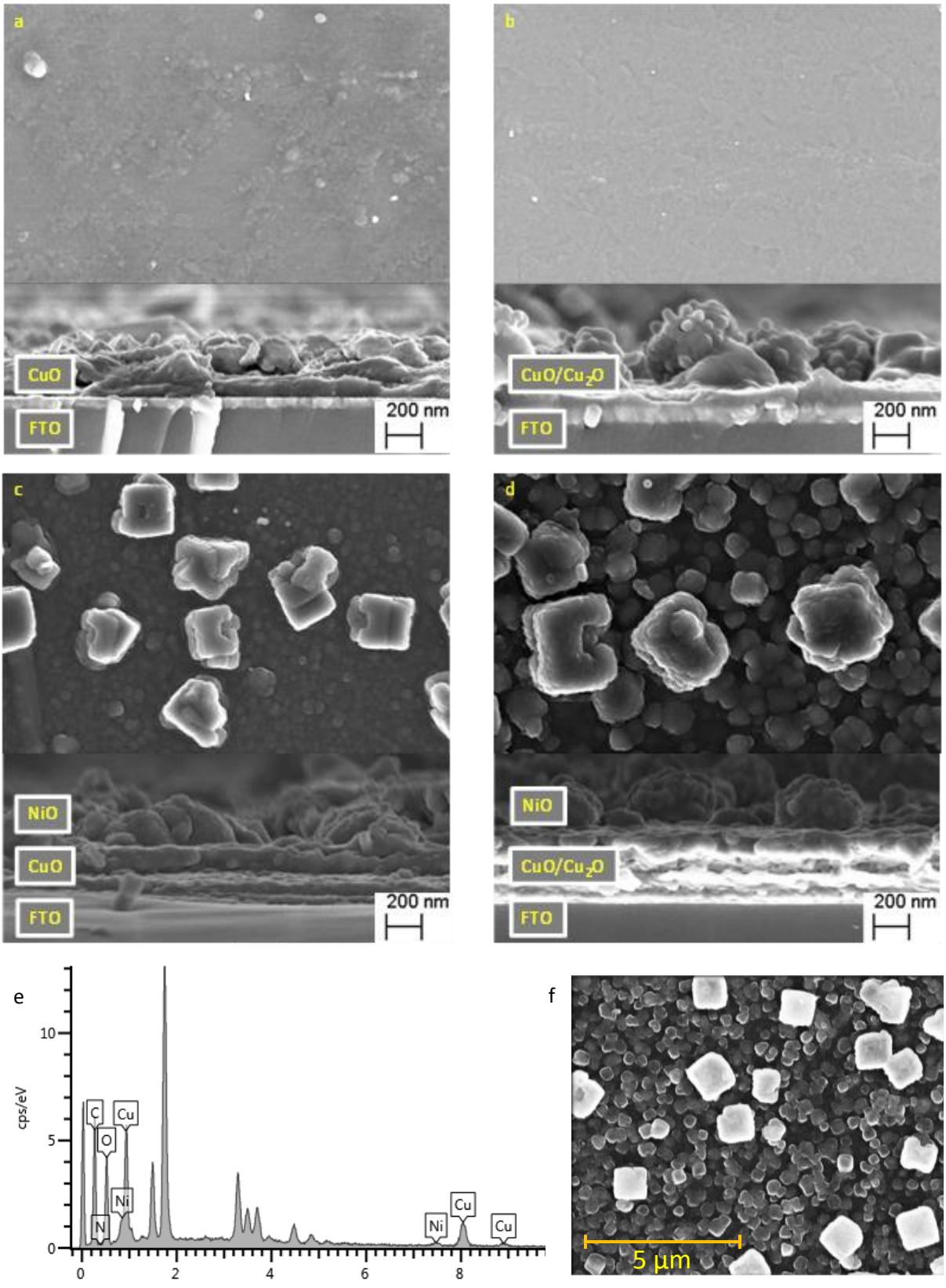

Figure 4-6 SEM images of top and cross-sectional area of a) CuO, b) N-CuO/Cu_2O, c) CuO:NiO, d) N-CuO/Cu_2O:NiO sensors, e) EDS spectrum of the N-CuO/Cu_2O:NiO sensor and f) area of the SEM image used for EDS measurements

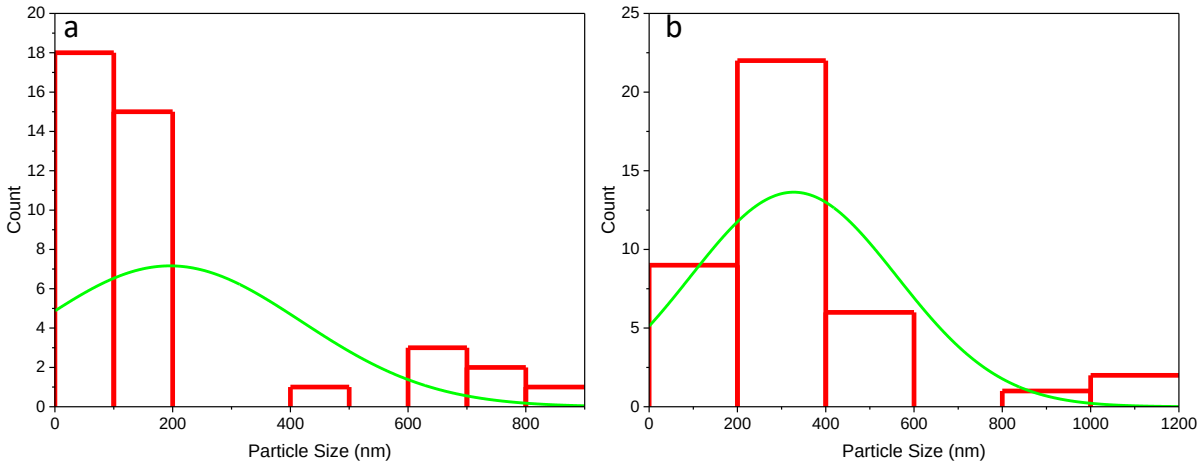

Figure 4-7 An average particle size distribution based on the SEM images of a) CuO:NiO and b) N-CuO/Cu_2O:NiO electrodes

4.1.4. Hall effect measurements

The carrier concentration and mobility of free electrons within an electroactive material can be determined using the Hall Effect technique (Werner, 2017, Gessert et al., 2011, Tyagi et al., 2012). Literature suggest that higher mobility is preferred as it results in a lower carrier concentration which produces less optical reflection and absorption (Gessert et al., 2011). The N-CuO/Cu_2O:NiO electrode demonstrates *N*-type semiconducting nature as a result of the negative bulk concentrations (Tyagi et al., 2012). The highest recorded electron mobility of CuO was 48.44 cm^2/Vs (Gao et al., 2019). In this work, the free electron mobility and conductivity of the N-CuO/Cu_2O:NiO electrode was 34.43 cm^2/Vs and 3187 1/Ωcm respectively. This is higher than the pristine CuO thin film (29.27 cm^2/Vs and 3030 1/Ωcm for free electron mobility and conductivity respectively). The improved mobility of this electrode may be a result of improved crystallinity and/or limited scattered centres for the charge carriers of the developed sensor (Tyagi et al., 2012).

4.2. Electrochemical evaluation of the N-CuO/Cu_2O:NiO thin film electrode

For the evaluation of the electrode, electrochemical evaluation was conducted using CV, EIS and chronoamperometry to determine the Tafel slopes, selectivity, repeatability, and the shelf life. These techniques are used to determine the performance of the electrode towards glucose oxidation. It also determined the effectiveness of the electrode towards glucose oxidation and thus can be compared to other glucose sensors.

4.2.1. Cyclic voltammetry (CV)

The electrochemical performance of the developed sensors towards the oxidation of glucose was evaluated using cyclic voltammetry (CV). CV experiments were conducted in alkaline solution of 0.1 M NaOH using a potential range from -0.1 V to 0.8 V vs Ag/AgCl at a scan rate of 25 mV/s (Zhang et al., 2014, Cheng et al., 2019). An alkaline solution of NaOH is used since carbohydrates such as glucose can be oxidised at high pH (Zhao et al., 2007). Experiments conducted by Zhang et al. (2013) suggest that an increase in NaOH in solution relates to an increase in peak current during glucose oxidation, due to the increased availability of hydroxyl radicals (OH^-) which are used in the glucose oxidation mechanism. Furthermore, the concentrations of 0.05 M and 0.1 M NaOH has a limited increase in oxidation peak current (Zhang et al., 2014). However, a 0.1 M NaOH was used due to the excess availability of OH^- ions (Zhang et al., 2014, Xiao et al., 2019, Cao et al., 2011). Electrodes prepared using the ratio of 70:30 (%V/V) copper to nickel precursor demonstrated the best electrochemical activity compared to the other ratios studied (Figure 4-8a). The improved electrochemical activity can be observed by increased oxidation current of the 30% Ni-solution CV diagram.

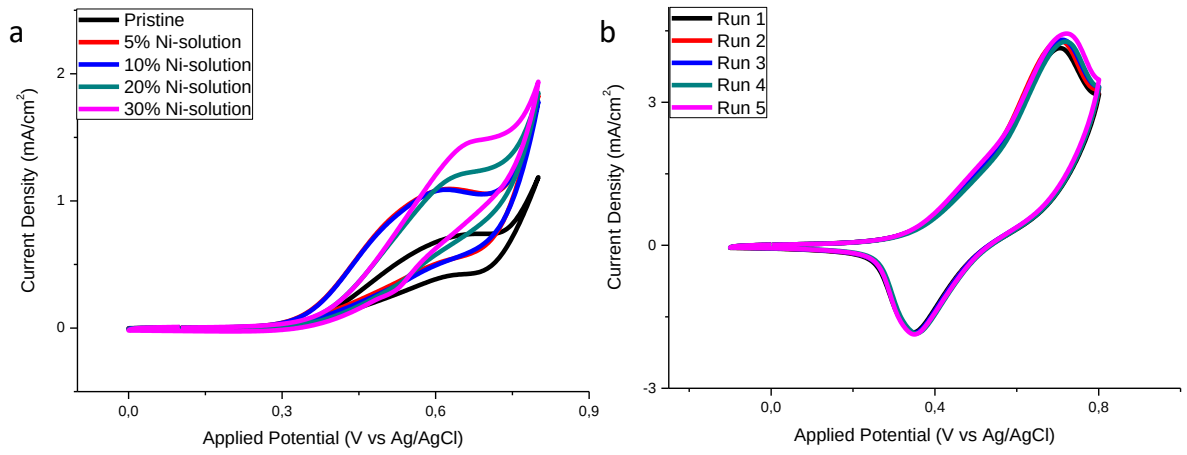

Figure 4-8 Cyclic voltammograms conducted at a scan rate of 25 mV/s for a) comparison of the effects of Ni composition on the peak oxidation current and b) repeatability of N-CuO/Cu_2O:NiO sensor in 1 mM glucose solution

The effect of film thickness (number of layer) on the electrochemical performance of the N-CuO/Cu_2O:NiO electrode prepared with 70:30 (%V/V) precursors was investigated with CV (Figure 4-9a) in the presence of 1 mM glucose. The result shows that with increasing film thickness the peak oxidation current of the electrode increases up to the fifth layer. With further addition of layers, no significant increase in the oxidation current was observed. Hence, only five-layer deposited N-CuO/Cu_2O:NiO electrodes were further evaluated. All results discussed from this point onward is for the aforementioned electrodes unless otherwise stated.

The electrochemical performance of pristine CuO, N-CuO/Cu_2O, CuO:NiO and N-CuO/Cu_2O:NiO, was probed using CV in both the absence and presence of 1 mM glucose in 0.1 M NaOH electrolyte solution at scan rate of 25 mV/s. In absence of glucose (Figure 4-9b), CuO and N-CuO/Cu_2O electrodes had no oxidation peak but presented a large oxidative tail due to the onset of water splitting inhibiting the CuO/CuOOH transition. In contrast the CuO:NiO and N-CuO/Cu_2O:NiO electrodes (Figure 4-9b), shows an oxidation peak at 0.56 mV and 0.60 mV for CuO:NiO and N-CuO/Cu_2O:NiO, respectively. In the reverse scan (Figure 4-9b), the CV shows a reduction peak and a broad peak for both electrodes. The cathodic peak at 0.37 mV and 0.34 mV represent the active dissolution of nickel (or NiOOH/NiO transition) (Iwueke et al., 2015) and broad cathodic peak at 0.617 mV and 0.60 mV assigned to CuOOH/CuO transition for CuO-NiO and N-CuO/Cu_2O:NiO, respectively. Compared with CuO and N-CuO/Cu_2O, the CuO:NiO and N-CuO/Cu_2O:NiO electrodes showed higher redox peak currents with N-CuO/Cu_2O:NiO electrode being the highest. The plasma assisted nitrogen doping and presence of NiO significantly increased the electrochemical activity of a CuO based electrode.

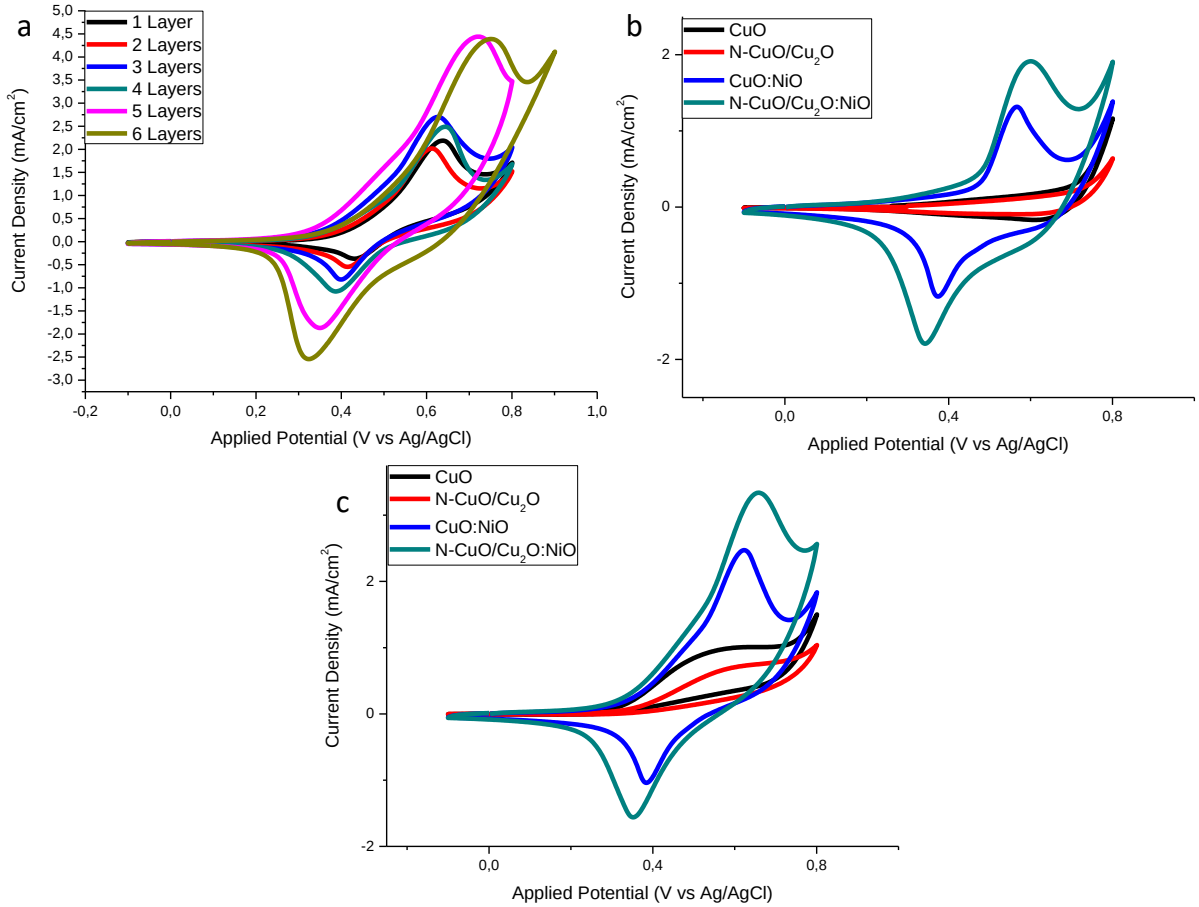

Figure 4-9 Cyclic Voltammogram scanned at 25 mV/s of a) increasing layers of the N-CuO/Cu_2O:NiO sensor, b) comparison of the sensor configurations (constant number of layers) in 0.1 M NaOH alone and c) comparison of the sensor configurations (constant number of layers) in 1 mM glucose

In the presence of 1 mM glucose, the four developed electrodes i.e., CuO, N-CuO/Cu_2O, CuO:NiO and N-CuO/Cu_2O:NiO were able to oxidise glucose (Figure 4-9c). An increase in peak current was observed in all cases. The pristine CuO electrode oxidises glucose at around 0.55 V. The following irreversible reactions show the electrocatalytic oxidation of glucose mechanism taking place on the CuO sensor (Cheng et al., 2019, Bai et al., 2017, Lin et al., 2018):

$$CuO + OH^- \rightarrow CuOOH + e^- \quad (2.15)$$

$$2CuOOH + glucose \rightarrow 2CuO + gluconolactone \quad (2.16)$$

Doping the CuO electrode with nitrogen decreased the oxidation peak current in Figure 4-9b and c. This can be attributed to the fact that the plasma treatment alone decreases surface roughness as was seen in the SEM images. From the results observed during XPS analysis, a predominant Cu_2O peak was present in the plasma treated CuO sensor, which has a direct effect on the oxidising ability of glucose. Literature suggests that CuO has improved electrooxidation capabilities compared to Cu_2O (Lin et al., 2018) which may have contributed to the lower glucose oxidation peak for N-CuO/Cu_2O compared to CuO as seen in Figure 4-9b and c. The mechanism used for the oxidation of glucose using mixed copper oxide can be described by the following equations (Lin et al., 2018):

$$Cu_2O + 2OH^- + H_2O \rightarrow 2Cu(OH)_2 + 2e^- \quad (2.13)$$

$$Cu(OH)_2 + OH^- \rightarrow CuOOH + H_2O + e^- \quad (2.14)$$

$$CuO + OH^- \rightarrow CuOOH + e^- \quad (2.15)$$

$$CuOOH + glucose \rightarrow Cu(OH)_2 + gluconolactone \quad (2.16)$$

Literature suggests that Cu^{3+} species act as the mediator for electron transferability during glucose oxidation. Glucose oxidation reaction require the presence of oxide, hydroxide and oxyhydroxide groups within an alkaline medium (Lin et al., 2018). The oxidation peak of the N-CuO/Cu_2O is observed at approximately 0.6 V. Thus, the N-CuO/Cu_2O electrode would behave as a catalyst during glucose oxidation, as seen in equations 2.13-2.16 (Lin et al., 2018). The glucose oxidation peak current for CuO:NiO electrode is significantly higher compared to pristine CuO and N-CuO/Cu_2O electrodes. However, the oxidation occurs at a slightly higher positive potential compared to the CuO and N-CuO/Cu_2O electrodes. The NiO species contribute to the glucose oxidation reaction through the following redox reaction (Zhu et al., 2018, Yi et al., 2015, Si et al., 2013):

$$NiO + OH^- \rightarrow Ni(OH)_2 \quad (2.10)$$

$$Ni(OH)_2 + OH^- \rightarrow NiOOH + H_2O + e^- \quad (2.11)$$

$$NiOOH + glucose \rightarrow Ni(OH)_2 + gluconolactone \quad (2.12)$$

The CuO:NiO electrode uses equations 2.10-2.12 and equations 2.15 and 2.16 during the electrooxidation of glucose which can be deduced by the peak observed at 0.62 V (Bai et al., 2017). Moreover, the presence of the NiO creates a multi-species composition which has a synergetic effect on the promotion of glucose oxidation (Chowdhury et al., 2017a, Cheng et al., 2019, Bai et al., 2017). Nitrogen doping the CuO:NiO film further improved the electroactivity of the electrode as observed in Figure 4-9b and c and the mechanism for the catalysation of glucose into gluconolactone is observed through equations 2.10-2.16. This mechanism for the electrooxidation of glucose is illustrated by the peak current at 0.67 V, which is greater than the experiments conducted by Bai et al. (2017). According to literature, the presence of nitrogen increases the applied potential required for the oxidation of glucose compared to the electrode without nitrogen (Yang et al., 2017a, Yang et al., 2017b). The improved electrocatalytic ability of the N-CuO/Cu_2O:NiO electrode may be the result of the an increase in catalytic active sites and a pair of electrons for conjugation, provided by the nitrogen's π-conjugated rings, introducing electron donor characteristics for the electrode (Yang et al., 2017b). Furthermore, this improved electroactivity is due to the enhanced electron transfer ability due to increase in electronic conductivity shown by the Hall effect measurement in section 4.1.4 (Gowthaman et al., 2017, Yang et al., 2017a). The glucose sensing ability of the N-CuO/Cu_2O:NiO electrode were evaluated by increasing glucose concentration from 1 mM to 5 mM (Figure 4-10a). The oxidation peak current increases significantly with increasing glucose concentration. At a glucose concentration of 5 mM, the response of the sensor to glucose started to reach saturation. To further understand the electrochemical behavior of the N-CuO/Cu_2O:NiO sensor, CV studies were performed in a 0.1 M NaOH solution containing 1 mM glucose at various scan rates. The anodic and cathodic current peaks increased with increasing scan rate, as shown in Figure 4-10b. In addition, the reduction potential shifts negatively and the oxidation potential shifts positively with increasing scan rate. The good linear relationship between the square root of the scan rate and the redox peak current would indicate a diffusion driven process which is a relatively fast (Chowdhury et al., 2017b, Bai et al., 2017, Ding et al., 2010) and reversible electron transfer reaction (Nicholson and Shain, 1964, Electrochemistry, 2000). This linear relationship can be observed in the inset of Figure 4-10b until 100 mV/s. However, at higher scan rates (200 mV/s) the reaction becomes too slow and equilibrium cannot be reached timeously, as the current takes longer to respond to the applied potential creating an irreversible electron transfer reaction (Electrochemistry, 2000, Nicholson and Shain, 1964).

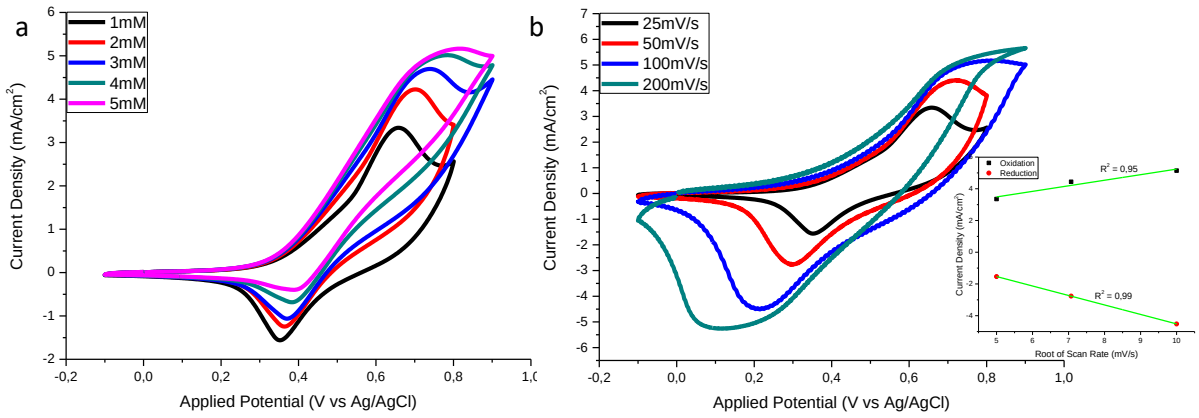

Figure 4-10 CV diagrams of the N-CuO/Cu_2O:NiO sensor with a) various concentrations of glucose at 25 mV/s and b) various scan rates with inset of linear relationship between square root of scan rate and peak current density

4.2.2. Tafel slope

To further understand the electrochemical performance of the N-CuO/Cu_2O:NiO electrode Tafel slopes of the developed electrodes were obtained in 0.1 M NaOH solution containing 1 mM glucose as shown in Figure 4-11. The Tafel slopes followed a trend as CuO > N-CuO/Cu_2O > CuO:NiO > N-CuO/Cu_2O:NiO. The lowest Tafel slope value of the N-CuO/Cu_2O:NiO electrode highlights that the plasma assisted nitrogen doping and presence of NiO increased the charge transferability of the material (Xu et al., 2017, Karim-Nezhad et al., 2009).

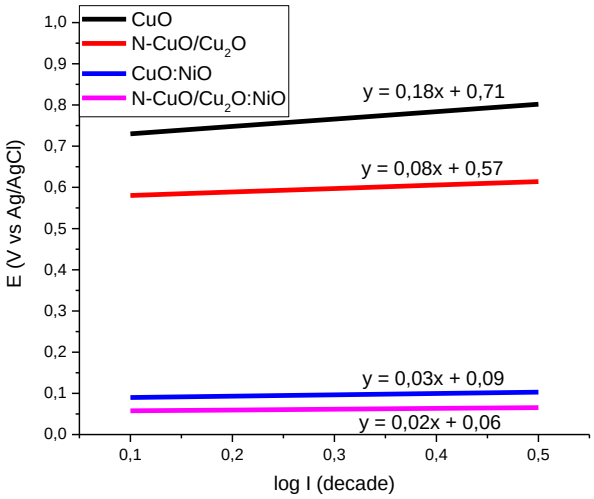

Figure 4-11 Tafel slopes of the developed electrodes in 0.1 M NaOH scanned at 25 mV/s

4.2.3. Electrochemical impedance spectroscopy (EIS)

EIS was used to further study the electrochemical characteristic of N-CuO/Cu_2O:NiO electrode. The Nyquist plot of the developed sensors are shown in Figure 4-12a and the fitted

data are in Figure 4-13. Included in this figure is the χ^2, indicating how well the data fits the equivalent electrical circuit and the percentage error of the corresponding R_{ct} value. The Nyquist plots exhibit two depressed semi-circles and a straight line in the low-frequency region. The semi-circle represented at higher frequencies region can be assigned to the double layered capacitance of the electrode-electrolyte interaction and the overall charge transfer resistance (R_{ct}) (MacDonald and Andreas, 2014, Li et al., 2015a) and the linear diffusion can be modelled using a Warburg impedance (W).

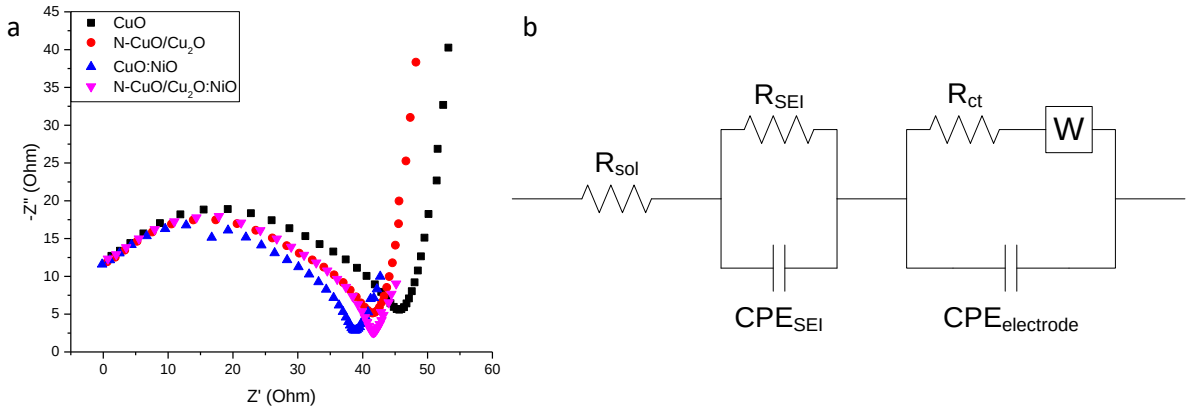

Figure 4-12 a) Nyquist plots of the CuO and N-CuO/Cu_2O:NiO sensors and b) Schematic of the equivalent circuit used for fitting

An equivalent electrical circuit proposed for fitting the data, related to the various developed sensors in 0.1 M NaOH, is shown in Figure 4-12b. This is an approximation of the complex plane system generated by the EIS experiments (MacDonald and Andreas, 2014, Choi et al., 2020). The charge transfer resistance (R_{ct}) quantifies the resistance to the flow of ions at the electrode and electrolyte interface (Li et al., 2015a). The R_{ct} values determined from the modelled equivalent electrical circuit are presented in Table 4-1. The results suggest that the CuO:NiO electrode has the lowest R_{ct} compared to the other electrodes. However, the N-CuO/Cu_2O:NiO exhibits a smaller R_{ct} value compared to the CuO and N-CuO/Cu_2O electrodes. A lower R_{ct} value indicates and easier flow of electrons due to smaller resistance (Li et al., 2015a). This result coupled with Hall effect and the Tafel plots discussed earlier demonstrates the enhance electrochemical performance of the N-CuO/Cu_2O:NiO electrode.

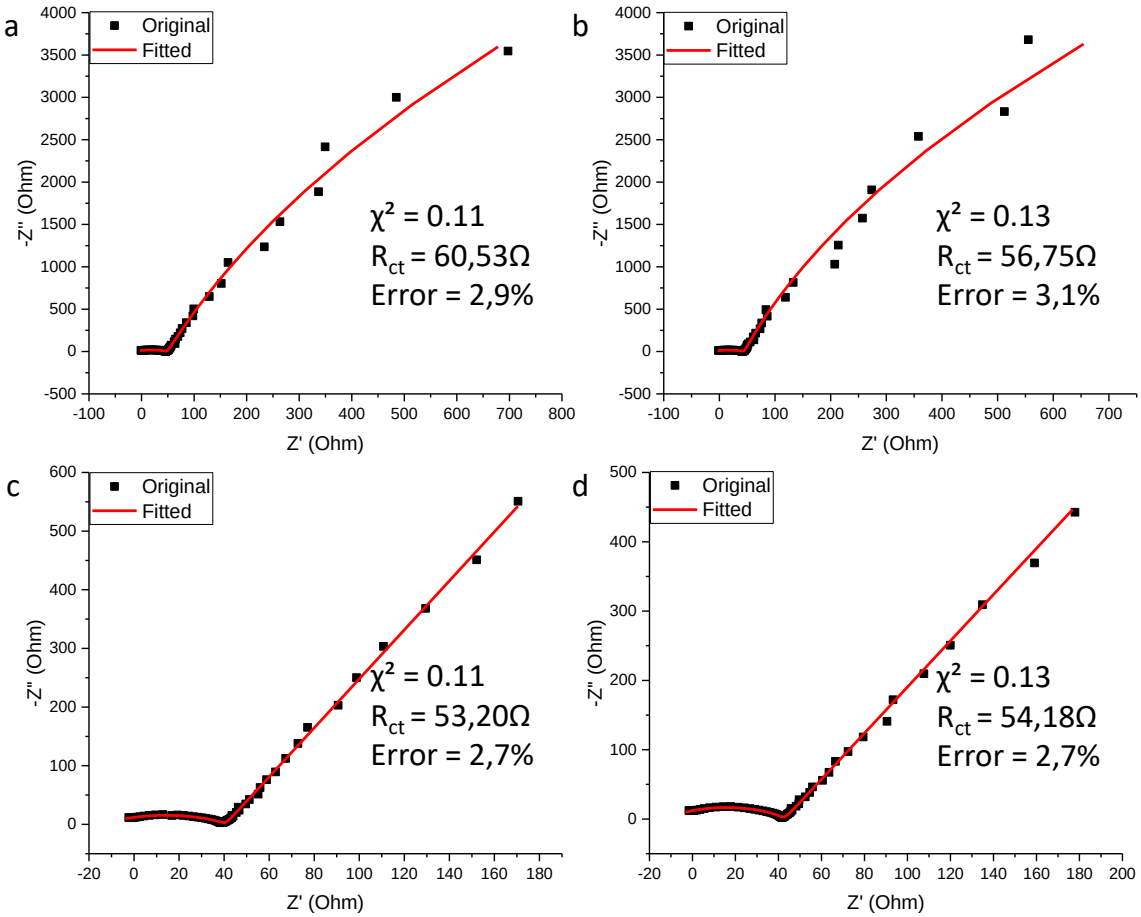

Figure 4-13 Fitted Nyquist plots of a) CuO, b) N-CuO/C_2O, c) CuO:NiO and d) N-CuO/Cu_2O:NiO electrodes

Table 4-1 Charge transfer resistance determined with equivalent circuit fitting for each developed sensor

Material	R_{ct} (Ω)	Estimated Error (%)
CuO	60.53	2.89
N-CuO/Cu_2O	56.75	3.11
CuO:NiO	53.20	2.71
N-CuO/Cu_2O:NiO	54.18	2.75

4.2.4. Chronoamperometric study of the N-CuO/Cu_2O:NiO electrode

Increasing concentration of glucose was added successively at an interval of 30s (Figure 4-14a) under stirring at a potential of 0.67 V in 0.1 M NaOH to evaluate the sensor performance (Chowdhury et al., 2017a, Ding et al., 2010). A typical step response (Yang et al., 2017a) was observed with a rapid response time of 2.5s towards successive additions of glucose. The dose response curve is presented in Figure 4-14b and can be quantified using the equation Current (I) = $1.131X_{conc}$ + 0.234 for the linear range of 0.05 – 2.74 mM of glucose with a

sensitivity of 1131 µA/mM.cm^2. The detection limit of the sensor was 21 µM. A comparison of the performance characteristics is provided in Table 4-2 for the developed sensors, showing the superiority in glucose sensing ability of the N-CuO/Cu_2O:NiO compared to the other developed sensors. The corresponding dosage response curves of the CuO, N-CuO/Cu_2O and CuO:NiO sensors is presented in Figure 4-15.

Table 4-2 Performance characteristics of the various developed sensors

Material	Sensitivity (µA/mM.cm^2)	Linear Range (mM)	LOD (mM)
CuO	830	0.05 - 1.65	0.022
N-CuO/Cu_2O	873	0.05 - 1.91	0.014
CuO:NiO	1103	0.05 - 1.65	0.061
N-CuO/Cu_2O:NiO	1131	0.05 - 2.74	0.020

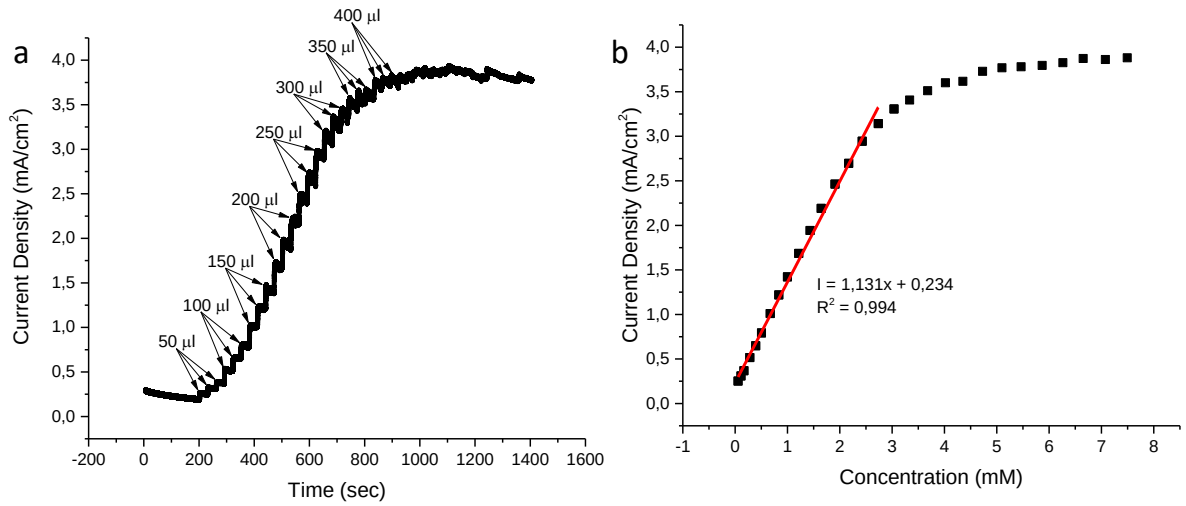

Figure 4-14 Amperometric response of the N-CuO/Cu_2O:NiO sensor to a) successive additions of glucose and b) corresponding calibration curve including the linear range

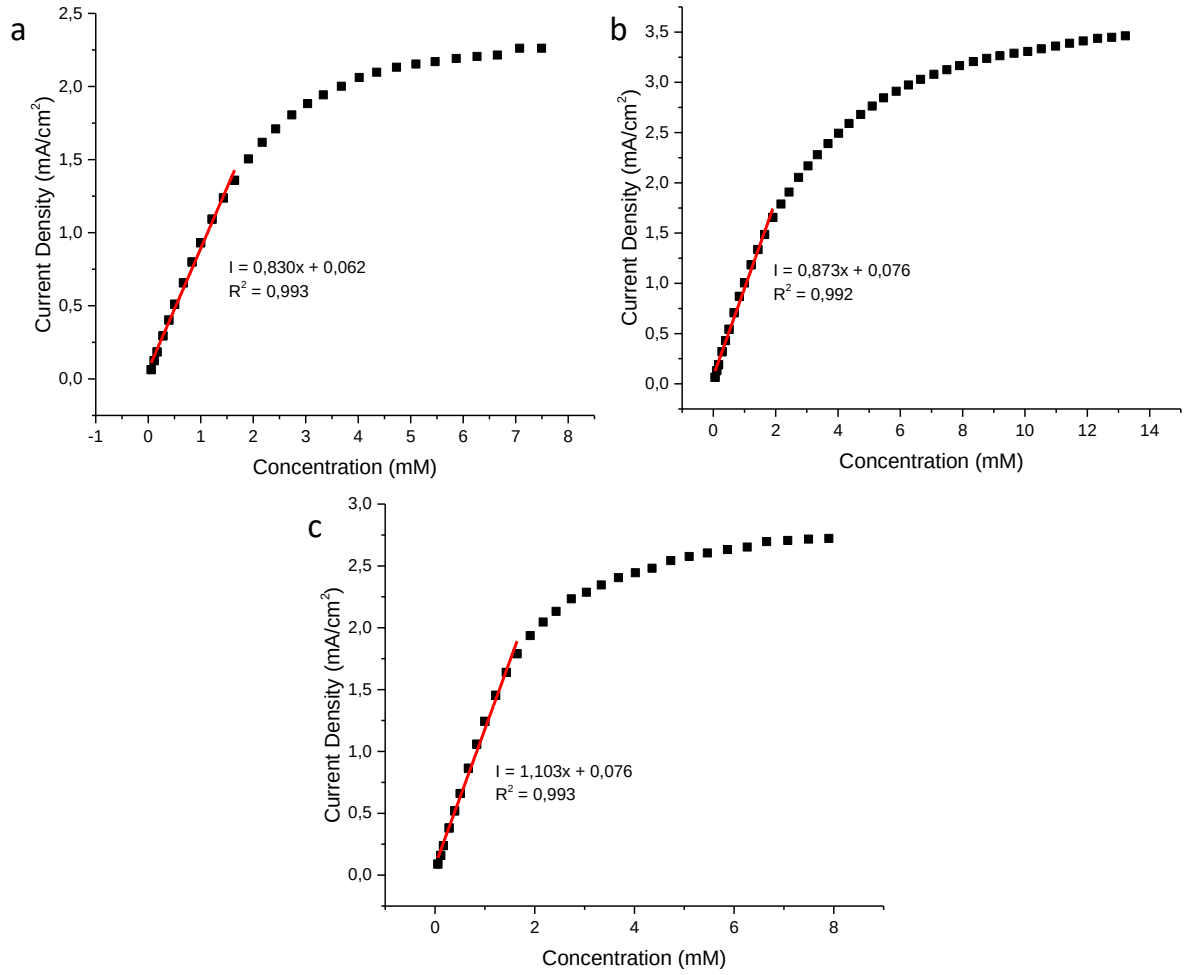

Figure 4-15 Amperometric dosage response curve of a) CuO, b) N-CuO/Cu_2O and c) CuO:NiO electrodes

4.2.5. Selectivity, repeatability, and shelf life

Selectivity, repeatability, and shelf life are important characteristics for practical application of the developed sensors (Yang et al., 2017a, Chowdhury et al., 2017a, Cheng et al., 2019). The selectivity of the electrode was performed in the presence of interference species i.e., uric acid, ascorbic acid, sucrose, and fructose (Figure 4-16a). Literature suggest that in physiological fluid i.e. blood, glucose concentrations are 10 times greater than the interference species mentioned above (Reach and Wilson, 1992, Ko et al., 2013). The selectivity was investigated with 200 µM of glucose and 20 µM of the interference species at the same applied potential used for the chronoamperometric sensing (Chowdhury et al., 2017a, Chowdhury et al., 2017b). The N-CuO/Cu_2O:NiO developed sensor was selective towards glucose at the specified potential showing minimal interference of other species. The N-CuO/Cu_2O:NiO sensor still showed a response to glucose after the successive additions of interference species (Figure 4-16a). The surface of the electrode is not poisoned by the presence of the interference species and is selective towards glucose. The sensor also showed response to

very low concentration (0.02mM) of human serum (Figure 4-16b). These findings demonstrate the potential of the as prepared electrode as a glucose sensor.

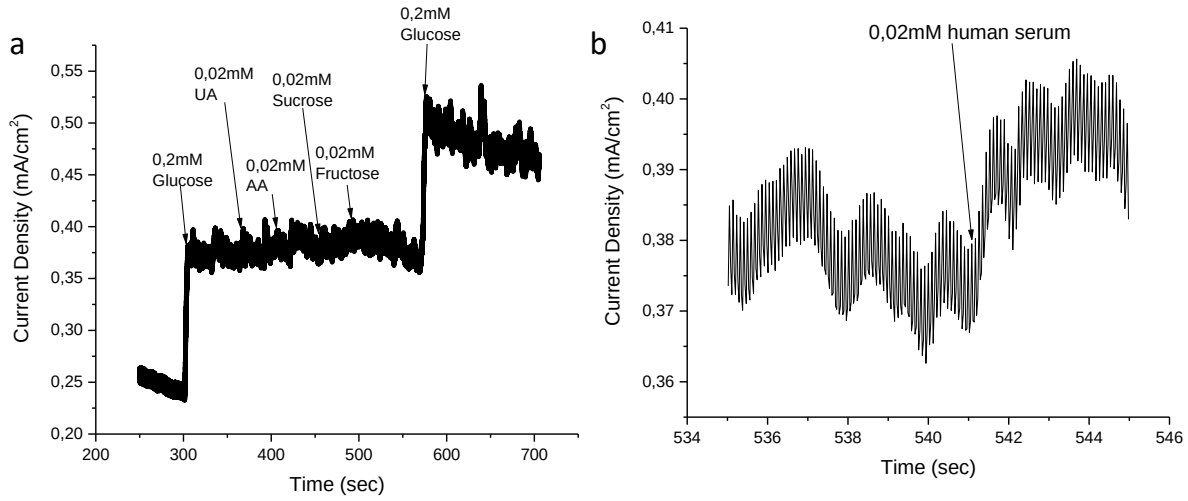

Figure 4-16 a) Selectivity test for interference species of biological samples and b) a magnification of an 0.02 mM injection of human serum

During the repeatability tests, the electrode is rinsed with deionized water and air dried using a compressed air blower, removing excess moisture and impurities, after each CV cycle. This procedure was repeated for five CV cycles and the results obtained were calculated accordingly. The developed sensor exhibited an RSD of less than 3% for the repeatability (Figure 4-8b), also it has an RSD of 16% over a 4-week period. These demonstrates high repeatability and stability of the N-CuO/Cu_2O:NiO sensor. The thin film of N-CuO/Cu_2O:NiO adheres to the FTO glass electrode after numerous CV cycles, rinsing in deionized water and dried with a compressed air blower. This excellent adhesion is shown by the minimal change of 3% in electrochemical oxidation of glucose during repeatability and 16% change for the stability tests. Also, no debris was seen floating in the electrolyte solution during the CV cycles. A comparison of the as prepared sensor performance with other non-enzymatic glucose sensors reported in the literature for glucose detection is presented Table 4-3. The electrochemical performance of the developed material is in par with the previous reported sensors.

Table 4-3 Comparison of the N-CuO/Cu_2O:NiO sensor with previously developed sensors

Material Used	Sensitivity ($\mu A/mM.cm^2$)	Linear Range (mM)	Reference
N-CuO/Cu_2O:NiO film	1131	0.05 – 2.74	this work
CuO doped NiO microfibres	3165	0.003 - 0.51	(Cao et al., 2011)
CuO nanowires	1800	up to 2	(Espro et al., 2014)
CuO nanofibres	431	0.006 - 2.5	(Wang et al., 2009)
CuO/Cu_2O nanofibres	830	up to 10	(Lu et al., 2014)
Ni doped ZrAlCo-O composite structure	1553	up to 2.8	(Wu et al., 2019)
Zn doped Co_3O_4 film	193	up to 0.62	(Chowdhury et al., 2017a)
Co_3O_4 film	398	0.021 - 1.74	(Gota et al., 2017)

CHAPTER 5: CONCLUSION AND RECOMMENDATIONS

5.1. Conclusion

A plasma assisted nitrogen doped mixed oxide, N-CuO/Cu_2O:NiO, sensor was developed through a binderless, solution-based process for biosensing applications. It may be concluded from the XRD results that the pristine host structure of the developed sensor consists of CuO. Furthermore, the introduction of Ni precursor created NiO nanostructures with the host structure of CuO. SEM images showed that the NiO was present in cube-like structures bonded with the CuO. The XPS data suggests that plasma assisted nitrogen doping induced phase conversion of CuO to Cu_2O. Plasma treatment also etched the surface reducing the surface roughness of the synthesised electrodes.

The recorded cyclic voltammograms showed that a ratio of 70:30 (%V/V) of Cu precursor to Ni precursor generates a favourable oxidation peak. Plasma treated copper oxide and nickel oxide composite structure, N-CuO/Cu_2O:NiO, exhibited the highest oxidation peak during glucose oxidation compared to the other materials developed in this study. The optimal electrode thickness was established in a layer study using the N-CuO/Cu_2O:NiO, showing that 5 layers produced the highest oxidation peak compared to 4 and 6 layers. The N-CuO/Cu_2O:NiO electrode exhibited the most favorable Tafel slope compared to the other developed sensors suggesting superior charge transferability. A favorable free electron mobility and conductivity of the N-CuO/Cu_2O:NiO sensor was achieved when compared to the pristine structure of CuO. The R_{ct} value of 54.18 Ω for the N-CuO/Cu_2O:NiO was similar to the CuO:NiO and far superior compared to the pristine CuO confirming the enhanced electronic properties of the developed sensor.

In this study, the greatest sensitivity of 1131 µA/mM.cm^2 and widest linear range of 0.05 – 2.74 mM of glucose was recorded with the N-CuO/Cu_2O:NiO sensor. These results illustrate the superiority of the N-CuO/Cu_2O:NiO compared to the other materials developed in this study. This study showed that the introduction of a composite material, i.e., NiO and CuO increased the electrochemical activity of the material and that plasma treatment increased the active surface area.

5.2. Recommendations

- ✓ The EIS experiments should be conducted on the different precursor ratios to analyse the charge transfer of the various sensors. This would aid in understanding the role NiO plays in the enhancements of electronic properties.
- ✓ Varied plasma treatment conditions should be used to determine a favourable doping of N into the catalytic material.
- ✓ Different composite structure could benefit from the introduction of N through plasma assisted doping, which would optimize the properties of the catalytic material.

REFERENCES

ADITHA, S. K., KURDEKAR, A. D., CHUNDURI, L. A., PATNAIK, S. & KAMISETTI, V. 2016. Aqueous based reflux method for green synthesis of nanostructures: Application in CZTS synthesis. *MethodsX,* 3**,** 35-42.

AL-OMAIR, M. A., TOUNY, A., AL-ODAIL, F. A. & SALEH, M. 2017. Electrocatalytic oxidation of glucose at nickel phosphate nano/micro particles modified electrode. *Electrocatalysis,* 8**,** 340-350.

ASSOCIATION, A. D. 2010. Diagnosis and classification of diabetes mellitus. *Diabetes care,* 33**,** S62-S69.

BAER, D. R. & THEVUTHASAN, S. 2010. Characterization of thin films and coatings. *Handbook of Deposition Technologies for Films and Coatings.* Elsevier.

BAGOTZKY, V. & VASSILYEV, Y. B. 1967. Mechanism of electro-oxidation of methanol on the platinum electrode. *Electrochimica Acta,* 12**,** 1323-1343.

BAI, X., CHEN, W., SONG, Y., ZHANG, J., GE, R., WEI, W., JIAO, Z. & SUN, Y. 2017. Nickel-copper oxide nanowires for highly sensitive sensing of glucose. *Applied Surface Science,* 420**,** 927-934.

BARD, A. J. & FAULKNER, L. R. 2001. Fundamentals and applications. *Electrochemical Methods,* 2**,** 580-632.

BIESINGER, M. C. 2017. Advanced analysis of copper X-ray photoelectron spectra. *Surface and Interface Analysis,* 49**,** 1325-1334.

BIESINGER, M. C., LAU, L. W., GERSON, A. R. & SMART, R. S. C. 2010. Resolving surface chemical states in XPS analysis of first row transition metals, oxides and hydroxides: Sc, Ti, V, Cu and Zn. *Applied surface science,* 257**,** 887-898.

BROSTER, P., CARTER, P. & JAMES, H. 2007. *Oxford successful physical sciences. Grade 12, Grade 12,* Cape Town, Oxford University Press Southern Africa.

BURKE, L. 1994. Premonolayer oxidation and its role in electrocatalysis. *Electrochimica Acta,* 39**,** 1841-1848.

CAO, F., GUO, S., MA, H., YANG, G., YANG, S. & GONG, J. 2011. Highly sensitive nonenzymatic glucose sensor based on electrospun copper oxide-doped nickel oxide composite microfibers. *Talanta,* 86**,** 214-220.

CARRÀ, S. 2018. *Stepping Stones to Synthetic Biology*, Springer.

CASH, K. J. & CLARK, H. A. 2010. Nanosensors and nanomaterials for monitoring glucose in diabetes. *Trends in molecular medicine,* 16**,** 584-593.

CHENG, S., DELACRUZ, S., CHEN, C., TANG, Z., SHI, T., CARRARO, C. & MABOUDIAN, R. 2019. Hierarchical Co3O4/CuO nanorod array supported on carbon cloth for highly sensitive non-enzymatic glucose biosensing. *Sensors and Actuators B: Chemical,* 298**,** 126860.

CHEREVKO, S. & CHUNG, C.-H. 2009. Gold nanowire array electrode for non-enzymatic voltammetric and amperometric glucose detection. *Sensors and Actuators B: Chemical,* 142**,** 216-223.

CHOI, W., SHIN, H.-C., KIM, J. M., CHOI, J.-Y. & YOON, W.-S. 2020. Modeling and Applications of Electrochemical Impedance Spectroscopy (EIS) for Lithium-ion Batteries. *Journal of Electrochemical Science and Technology,* 11**,** 1-13.

CHOPRA, P. & KUMAR, T. 2011. Correlation of glucose level among venous, gingival and finger-prick blood samples in diabetic patients. *Journal of Indian Society of Periodontology,* 15**,** 288.

CHOWDHURY, M., CUMMINGS, F., KEBEDE, M. & FESTER, V. 2017a. Binderless Solution Processed Zn Doped Co3O4 Film on FTO for Rapid and Selective Non-enzymatic Glucose Detection. *Electroanalysis,* 29**,** 578-586.

CHOWDHURY, M., OSSINGA, C., CUMMINGS, F., CHAMIER, J. & KEBEDE, M. 2017b. Novel Sn Doped Co3O4 Thin Film for Nonenzymatic Glucose Bio-Sensor and Fuel Cell. *Electroanalysis,* 29**,** 1876-1886.

COSNIER, S., LE GOFF, A. & HOLZINGER, M. 2014. Towards glucose biofuel cells implanted in human body for powering artificial organs: Review. *Electrochemistry Communications,* 38**,** 19-23.

DAR, M., KIM, Y., KIM, W., SOHN, J. & SHIN, H. 2008. Structural and magnetic properties of CuO nanoneedles synthesized by hydrothermal method. *Applied Surface Science,* 254**,** 7477-7481.

DHARA, K., RAMACHANDRAN, T., NAIR, B. G. & BABU, T. S. 2015. Single step synthesis of Au–CuO nanoparticles decorated reduced graphene oxide for high performance disposable nonenzymatic glucose sensor. *Journal of Electroanalytical Chemistry,* 743**,** 1-9.

DING, Y., WANG, Y., SU, L., BELLAGAMBA, M., ZHANG, H. & LEI, Y. 2010. Electrospun Co3O4 nanofibers for sensitive and selective glucose detection. *Biosensors and Bioelectronics,* 26**,** 542-548.

DONG, X.-C., XU, H., WANG, X.-W., HUANG, Y.-X., CHAN-PARK, M. B., ZHANG, H., WANG, L.-H., HUANG, W. & CHEN, P. 2012. 3D graphene–cobalt oxide electrode for high-performance supercapacitor and enzymeless glucose detection. *ACS nano,* 6**,** 3206-3213.

DONNELLY, V. M. & KORNBLIT, A. 2013. Plasma etching: Yesterday, today, and tomorrow. *Journal of Vacuum Science & Technology A: Vacuum, Surfaces, and Films,* 31**,** 050825.

DU, Y., ZHANG, W. & WANG, M. L. 2016. Sensing of Salivary Glucose Using Nano-Structured Biosensors. *Biosensors,* 6**,** 10.

ELECTROCHEMISTRY, A. 2000. Ed. J. Wang. Wiley VCH, New York.

ENGELHARD, M. H., DROUBAY, T. C. & DU, Y. 2017. X-ray photoelectron spectroscopy applications. Pacific Northwest National Laboratory (PNNL), Richland, WA (US ….

ESPRO, C., DONATO, N., GALVAGNO, S., ALOISIO, D., LEONARDI, S. G. & NERI, G. 2014. CuO nanowires-based electrodes for glucose sensors. *Chem. Eng,* 41.

ESWAR, N. K., GUPTA, R., RAMAMURTHY, P. C. & MADRAS, G. 2018. Influence of copper oxide grown on various conducting substrates towards improved performance for photoelectrocatalytic bacterial inactivation. *Molecular Catalysis,* 451**,** 161-169.

FASMIN, F. & SRINIVASAN, R. 2017. Nonlinear electrochemical impedance spectroscopy. *Journal of The Electrochemical Society,* 164**,** H443-H455.

FELDMAN, B., MCGARRAUGH, G., HELLER, A., BOHANNON, N., SKYLER, J., DELEEUW, E. & CLARKE, D. 2000. FreeStyle™: a small-volume electrochemical glucose sensor for home blood glucose testing. *Diabetes technology & therapeutics,* 2**,** 221-229.

GAO, X., DU, Y. & MENG, X. 2019. Cupric oxide film with a record hole mobility of 48.44 cm2/Vs via direct–current reactive magnetron sputtering for perovskite solar cell application. *Solar Energy,* 191**,** 205-209.

GESSERT, T., BURST, J., LI, X., SCOTT, M. & COUTTS, T. 2011. Advantages of transparent conducting oxide thin films with controlled permittivity for thin film photovoltaic solar cells. *Thin Solid Films,* 519**,** 7146-7148.

GLOAGUEN, F., ANDOLFATTO, F., DURAND, R. & OZIL, P. 1994. Kinetic study of electrochemical reactions at catalyst-recast ionomer interfaces from thin active layer modelling. *Journal of Applied Electrochemistry,* 24**,** 863-869.

GOLDSTEIN, J. I., NEWBURY, D. E., ECHLIN, P., JOY, D. C., LYMAN, C. E., LIFSHIN, E., SAWYER, L. & MICHAEL, J. R. 2003. Quantitative X-ray analysis: the basics. *Scanning Electron Microscopy and X-ray Microanalysis.* Springer.

GOTA, T., CHOWDHURY, M. & OJUMU, T. 2017. Non-enzymatic Fructose Sensor Based on Co3O4 Thin Film. *Electroanalysis,* 29**,** 2855-2862.

GOWTHAMAN, N., RAJ, M. A. & JOHN, S. A. 2017. Nitrogen-doped graphene as a robust scaffold for the homogeneous deposition of copper nanostructures: A nonenzymatic disposable glucose sensor. *ACS Sustainable Chemistry & Engineering,* 5**,** 1648-1658.

GUO, Y., LIU, J., XU, Y.-T., ZHAO, B., WANG, X., FU, X.-Z., SUN, R. & WONG, C.-P. 2019. In situ redox growth of mesoporous Pd-Cu2O nanoheterostructures for improved glucose oxidation electrocatalysis. *Science Bulletin*.

HOVANCOVÁ, J., NIŠČÁKOVÁ, V., ŠIŠOLÁKOVÁ, I., ORIŇAKOVÁ, R., MASKAĽOVÁ, I., ORIŇAK, A. & KOVAĽ, K. 2020. Gold Microelectrodes Decorated by Spike-Like Nanostructures as a Promising Non-Enzymatic Glucose Sensor. *Electroanalysis*.

HSU, Y.-W., HSU, T.-K., SUN, C.-L., NIEN, Y.-T., PU, N.-W. & GER, M.-D. 2012. Synthesis of CuO/graphene nanocomposites for nonenzymatic electrochemical glucose biosensor applications. *Electrochimica Acta,* 82**,** 152-157.

HUANG, T.-K., LIN, K.-W., TUNG, S.-P., CHENG, T.-M., CHANG, I.-C., HSIEH, Y.-Z., LEE, C.-Y. & CHIU, H.-T. 2009. Glucose sensing by electrochemically grown copper nanobelt electrode. *Journal of Electroanalytical Chemistry,* 636**,** 123-127.

IWUEKE, D., AMAECHI, C., NWANYA, A., EKWEALOR, A., ASOGWA, P., OSUJI, R., MAAZA, M. & EZEMA, F. 2015. A novel chemical preparation of Ni (OH) 2/CuO nanocomposite thin films for supercapacitive applications. *Journal of Materials Science: Materials in Electronics,* 26**,** 2236-2242.

JIA, H., SHANG, N., FENG, Y., YE, H., ZHAO, J., WANG, H., WANG, C. & ZHANG, Y. 2020. Facile preparation of Ni nanoparticle embedded on mesoporous carbon nanorods for non-enzymatic glucose detection. *Journal of Colloid and Interface Science,* 583**,** 310-320.

JIANG, D., LIU, Q., WANG, K., QIAN, J., DONG, X., YANG, Z., DU, X. & QIU, B. 2014. Enhanced non-enzymatic glucose sensing based on copper nanoparticles decorated nitrogen-doped graphene. *Biosensors and Bioelectronics,* 54**,** 273-278.

KABIR, S., ARTYUSHKOVA, K., SEROV, A., KIEFER, B. & ATANASSOV, P. 2016. Binding energy shifts for nitrogen-containing graphene-based electrocatalysts–experiments and DFT calculations. *Surface and Interface Analysis,* 48**,** 293-300.

KARIM-NEZHAD, G., JAFARLOO, R. & DORRAJI, P. S. 2009. Copper (hydr) oxide modified copper electrode for electrocatalytic oxidation of hydrazine in alkaline media. *Electrochimica acta,* 54**,** 5721-5726.

KIM, D.-M. & SHIM, Y.-B. 2013. Disposable amperometric glycated hemoglobin sensor for the finger prick blood test. *Analytical chemistry,* 85**,** 6536-6543.

KO, C.-Y., HUANG, J.-H., RAINA, S. & KANG, W. P. 2013. A high performance non-enzymatic glucose sensor based on nickel hydroxide modified nitrogen-incorporated nanodiamonds. *Analyst,* 138**,** 3201-3208.

KOHLI, R. & MITTAL, K. Developments in Surface Contamination and Cleaning, Volumes 1–12. Elsevier.

KUNG, C.-W., LIN, C.-Y., LAI, Y.-H., VITTAL, R. & HO, K.-C. 2011. Cobalt oxide acicular nanorods with high sensitivity for the non-enzymatic detection of glucose. *Biosensors and Bioelectronics,* 27**,** 125-131.

KURNIAWAN, F., TSAKOVA, V. & MIRSKY, V. M. 2006. Gold nanoparticles in nonenzymatic electrochemical detection of sugars. *Electroanalysis: An International Journal Devoted to Fundamental and Practical Aspects of Electroanalysis,* 18**,** 1937-1942.

LI, X., LUO, D., ZHANG, X. & ZHANG, Z. 2015a. Enhancement of electrochemical performances for LiFePO4/C with 3D-grape-bunch structure and selection of suitable equivalent circuit for fitting EIS results. *Journal of Power Sources,* 291**,** 75-84.

LI, Z., XIN, Y., ZHANG, Z., WU, H. & WANG, P. 2015b. Rational design of binder-free noble metal/metal oxide arrays with nanocauliflower structure for wide linear range nonenzymatic glucose detection. *Scientific reports,* 5**,** 10617.

LIN, L.-Y., KARAKOCAK, B. B., KAVADIYA, S., SOUNDAPPAN, T. & BISWAS, P. 2018. A highly sensitive non-enzymatic glucose sensor based on Cu/Cu2O/CuO ternary composite hollow spheres prepared in a furnace aerosol reactor. *Sensors and Actuators B: Chemical,* 259**,** 745-752.

LIU, S., HUI, K. & HUI, K. 2016. Flower-like copper cobaltite nanosheets on graphite paper as high-performance supercapacitor electrodes and enzymeless glucose sensors. *ACS applied materials & interfaces,* 8**,** 3258-3267.

LIU, Y., TENG, H., HOU, H. & YOU, T. 2009. Nonenzymatic glucose sensor based on renewable electrospun Ni nanoparticle-loaded carbon nanofiber paste electrode. *Biosensors and Bioelectronics,* 24**,** 3329-3334.

LU, L.-M., ZHANG, L., QU, F.-L., LU, H.-X., ZHANG, X.-B., WU, Z.-S., HUAN, S.-Y., WANG, Q.-A., SHEN, G.-L. & YU, R.-Q. 2009. A nano-Ni based ultrasensitive nonenzymatic electrochemical sensor for glucose: enhancing sensitivity through a nanowire array strategy. *Biosensors and Bioelectronics,* 25**,** 218-223.

LU, N., SHAO, C., LI, X., SHEN, T., ZHANG, M., MIAO, F., ZHANG, P., ZHANG, X., WANG, K. & ZHANG, Y. 2014. CuO/Cu 2 O nanofibers as electrode materials for non-enzymatic glucose sensors with improved sensitivity. *Rsc Advances,* 4**,** 31056-31061.

LUO, X., MORRIN, A., KILLARD, A. J. & SMYTH, M. R. 2006. Application of Nanoparticles in Electrochemical Sensors and Biosensors. *Electroanalysis,* 18**,** 319-326.

MA, Y., DI, J., YAN, X., ZHAO, M., LU, Z. & TU, Y. 2009. Direct electrodeposition of gold nanoparticles on indium tin oxide surface and its application. *Biosensors and Bioelectronics,* 24**,** 1480-1483.

MACDONALD, M. A. & ANDREAS, H. A. 2014. Method for equivalent circuit determination for electrochemical impedance spectroscopy data of protein adsorption on solid surfaces. *Electrochimica Acta,* 129**,** 290-299.

MANYASREE, D., PEDDI, K. & RAVIKUMAR, R. 2017. CuO nanoparticles: synthesis, characterization and their bactericidal efficacy. *Int J Appl Pharmaceut,* 9**,** 71-74.

MASUDY-PANAH, S., RADHAKRISHNAN, K., KUMAR, A., WONG, T. I., YI, R. & DALAPATI, G. K. 2015. Optical bandgap widening and phase transformation of nitrogen doped cupric oxide. *Journal of Applied Physics,* 118**,** 225301.

MATANOVIC, I., ARTYUSHKOVA, K., STRAND, M. B., DZARA, M. J., PYLYPENKO, S. & ATANASSOV, P. 2016. Core level shifts of hydrogenated pyridinic and pyrrolic nitrogen in the nitrogen-containing graphene-based electrocatalysts: In-plane vs edge defects. *The Journal of Physical Chemistry C,* 120**,** 29225-29232.

MATHER, R. 2009. Surface modification of textiles by plasma treatments. *Surface modification of textiles.* Elsevier.

MCCORMICK, W. & MCCRUDDEN, D. 2020. Development of a highly nanoporous platinum screen-printed electrode and its application in glucose sensing. *Journal of Electroanalytical Chemistry,* 860**,** 113912.

MOUSAVI, P., HARAN, F., JEZ, D., SANTOSA, F. & DODGE, J. S. 2009. Simultaneous composition and thickness measurement of paper using terahertz time-domain spectroscopy. *Applied Optics,* 48**,** 6541-6546.

MU, Y., JIA, D., HE, Y., MIAO, Y. & WU, H.-L. 2011. Nano nickel oxide modified non-enzymatic glucose sensors with enhanced sensitivity through an electrochemical process strategy at high potential. *Biosensors and Bioelectronics,* 26**,** 2948-2952.

MUTHUSANKAR, G., SASIKUMAR, R., CHEN, S.-M., GOPU, G., SENGOTTUVELAN, N. & RWEI, S.-P. 2018. Electrochemical synthesis of nitrogen-doped carbon quantum dots decorated copper oxide for the sensitive and selective detection of non-steroidal anti-inflammatory drug in berries. *Journal of colloid and interface science,* 523**,** 191-200.

NICHOLSON, R. S. & SHAIN, I. 1964. Theory of stationary electrode polarography. Single scan and cyclic methods applied to reversible, irreversible, and kinetic systems. *Analytical chemistry,* 36**,** 706-723.

PARK, J., AN, K., HWANG, Y., PARK, J.-G., NOH, H.-J., KIM, J.-Y., PARK, J.-H., HWANG, N.-M. & HYEON, T. 2004. Ultra-large-scale syntheses of monodisperse nanocrystals. *Nature materials,* 3**,** 891.

PARK, S., CHUNG, T. D. & KIM, H. C. 2003. Nonenzymatic glucose detection using mesoporous platinum. *Analytical Chemistry,* 75**,** 3046-3049.

PLETCHER, D. 1984. Electrocatalysis: present and future. *Journal of applied electrochemistry,* 14**,** 403-415.

RAUF, S., HAYAT NAWAZ, M. A., BADEA, M., MARTY, J. L. & HAYAT, A. 2016. Nano-Engineered Biomimetic Optical Sensors for Glucose Monitoring in Diabetes. *Sensors,* 16**,** 1931.

REACH, G. & WILSON, G. S. 1992. Can continuous glucose monitoring be used for the treatment of diabetes. *Analytical chemistry,* 64**,** 381A-386A.

ROGLIC, G. 2016. WHO Global report on diabetes: A summary. *International Journal of Noncommunicable Diseases,* 1**,** 3.
SCOGNAMIGLIO, V. 2013. *Nanotechnology in Glucose Monitoring: Advances and Challenges in the Last 10 years*.
SHEN, P. & XIA, Y. 2014. Synthesis-modification integration: one-step fabrication of boronic acid functionalized carbon dots for fluorescent blood sugar sensing. *Analytical chemistry,* 86**,** 5323-5329.
SHEN, Q., JIANG, L., ZHANG, H., MIN, Q., HOU, W. & ZHU, J.-J. 2008. Three-dimensional dendritic Pt nanostructures: sonoelectrochemical synthesis and electrochemical applications. *The Journal of Physical Chemistry C,* 112**,** 16385-16392.
SI, P., HUANG, Y., WANG, T. & MA, J. 2013. Nanomaterials for electrochemical non-enzymatic glucose biosensors. *RSC Advances,* 3**,** 3487-3502.
SONG, H., NI, Y. & KOKOT, S. 2015. A novel electrochemical sensor based on the copper-doped copper oxide nano-particles for the analysis of hydrogen peroxide. *Colloids and Surfaces A: Physicochemical and Engineering Aspects,* 465**,** 153-158.
SOTO, G., DE LA CRUZ, W. & FARıAS, M. 2004. XPS, AES, and EELS characterization of nitrogen-containing thin films. *Journal of Electron Spectroscopy and Related Phenomena,* 135**,** 27-39.
TEE, S. Y., TENG, C. P. & YE, E. 2017. Metal nanostructures for non-enzymatic glucose sensing. *Materials Science and Engineering: C,* 70**,** 1018-1030.
TIAN, H., JIA, M., ZHANG, M. & HU, J. 2013. Nonenzymatic glucose sensor based on nickel ion implanted-modified indium tin oxide electrode. *Electrochimica Acta,* 96**,** 285-290.
TOGHILL, K. E. & COMPTON, R. G. 2010. Electrochemical non-enzymatic glucose sensors: a perspective and an evaluation. *Int. J. Electrochem. Sci,* 5**,** 1246-1301.
TOGHILL, K. E., XIAO, L., PHILLIPS, M. A. & COMPTON, R. G. 2010. The non-enzymatic determination of glucose using an electrolytically fabricated nickel microparticle modified boron-doped diamond electrode or nickel foil electrode. *Sensors and Actuators B: Chemical,* 147**,** 642-652.
TYAGI, M., TOMAR, M. & GUPTA, V. 2012. Influence of hole mobility on the response characteristics of p-type nickel oxide thin film based glucose biosensor. *Analytica chimica acta,* 726**,** 93-101.
UCHIC, M. D., HOLZER, L., INKSON, B. J., PRINCIPE, E. L. & MUNROE, P. 2007. Three-dimensional microstructural characterization using focused ion beam tomography. *MRS bulletin,* 32**,** 408-416.
VASSILYEV, Y. B., KHAZOVA, O. & NIKOLAEVA, N. 1985. Kinetics and mechanism of glucose electrooxidation on different electrode-catalysts: Part I. Adsorption and oxidation on platinum. *Journal of electroanalytical chemistry and interfacial electrochemistry,* 196**,** 105-125.
VISHWAKARMA, V. & UTHAMAN, S. 2020. Environmental impact of sustainable green concrete. *Smart Nanoconcretes and Cement-Based Materials.* Elsevier.
WAGNER, A. J., WOLFE, G. M. & FAIRBROTHER, D. H. 2003a. Reactivity of vapor-deposited metal atoms with nitrogen-containing polymers and organic surfaces studied by in situ XPS. *Applied surface science,* 219**,** 317-328.
WAGNER, C., NAUMKIN, A., KRAUT-VASS, A., ALLISON, J., POWELL, C. & RUMBLE JR, J. 2003b. NIST X-ray Photoelectron Spectroscopy Database, NIST Standard Reference Database 20, Version 3.4 (Web Version). *U. S. Department of Commerce.*
WANG, G., HE, X., WANG, L., GU, A., HUANG, Y., FANG, B., GENG, B. & ZHANG, X. 2013. Non-enzymatic electrochemical sensing of glucose. *Microchimica Acta,* 180**,** 161-186.
WANG, J., THOMAS, D. F. & CHEN, A. 2008. Nonenzymatic electrochemical glucose sensor based on nanoporous PtPb networks. *Analytical Chemistry,* 80**,** 997-1004.
WANG, W., ZHANG, L., TONG, S., LI, X. & SONG, W. 2009. Three-dimensional network films of electrospun copper oxide nanofibers for glucose determination. *Biosensors and Bioelectronics,* 25**,** 708-714.
WERNER, F. 2017. Hall measurements on low-mobility thin films. *Journal of Applied Physics,* 122**,** 135306.

WILLIAMS, R., COLAGIURI, S., CHAN, J., GREGG, E., KE, C., LIM, L.-L. & YANG, X. 2019. *IDF Atlas 9th Edition 2019*.

WU, X., CHEN, F., HUANG, M., DAN, Z. & QIN, F. 2019. Ni-decorated ZrAlCo-O nanotube arrays with ultrahigh sensitivity for non-enzymatic glucose sensing. *Electrochimica Acta*.

XIAO, X., PENG, S., WANG, C., CHENG, D., LI, N., DONG, Y., LI, Q., WEI, D., LIU, P. & XIE, Z. 2019. Metal/metal oxide@ carbon composites derived from bimetallic Cu/Ni-based MOF and their electrocatalytic performance for glucose sensing. *Journal of Electroanalytical Chemistry*.

XU, L., WANG, Z., WANG, J., XIAO, Z., HUANG, X., LIU, Z. & WANG, S. 2017. N-doped nanoporous Co3O4 nanosheets with oxygen vacancies as oxygen evolving electrocatalysts. *Nanotechnology,* 28**,** 165402.

YANG, J., TAN, W., CHEN, C., TAO, Y., QIN, Y. & KONG, Y. 2017a. Nonenzymatic glucose sensing by CuO nanoparticles decorated nitrogen-doped graphene aerogel. *Materials Science and Engineering: C,* 78**,** 210-217.

YANG, S., LI, G., WANG, D., QIAO, Z. & QU, L. 2017b. Synthesis of nanoneedle-like copper oxide on N-doped reduced graphene oxide: a three-dimensional hybrid for nonenzymatic glucose sensor. *Sensors and Actuators B: Chemical,* 238**,** 588-595.

YI, W., LIU, J., CHEN, H., GAO, Y. & LI, H. 2015. Copper/nickel nanoparticle decorated carbon nanotubes for nonenzymatic glucose biosensor. *Journal of Solid State Electrochemistry,* 19**,** 1511-1521.

YOON, H. 2013. Current Trends in Sensors Based on Conducting Polymer Nanomaterials. *Nanomaterials,* 3**,** 524-549.

YUAN, J., WANG, K. & XIA, X. 2005. Highly ordered platinum-nanotubule arrays for amperometric glucose sensing. *Advanced Functional Materials,* 15**,** 803-809.

ZHANG, W., DU, Y. & WANG, M. L. 2015. Noninvasive glucose monitoring using saliva nano-biosensor. *Sensing and Bio-Sensing Research,* 4**,** 23-29.

ZHANG, Y., LIU, Y., SU, L., ZHANG, Z., HUO, D., HOU, C. & LEI, Y. 2014. CuO nanowires based sensitive and selective non-enzymatic glucose detection. *Sensors and Actuators B: Chemical,* 191**,** 86-93.

ZHANG, Y., SU, L., MANUZZI, D., DE LOS MONTEROS, H. V. E., JIA, W., HUO, D., HOU, C. & LEI, Y. 2012a. Ultrasensitive and selective non-enzymatic glucose detection using copper nanowires. *Biosensors and Bioelectronics,* 31**,** 426-432.

ZHANG, Y., WANG, Y., JIA, J. & WANG, J. 2012b. Nonenzymatic glucose sensor based on graphene oxide and electrospun NiO nanofibers. *Sensors and Actuators B: Chemical,* 171**,** 580-587.

ZHAO, C., SHAO, C., LI, M. & JIAO, K. 2007. Flow-injection analysis of glucose without enzyme based on electrocatalytic oxidation of glucose at a nickel electrode. *Talanta,* 71**,** 1769-1773.

ZHENG, S., LI, B., TANG, Y., LI, Q., XUE, H. & PANG, H. 2018. Ultrathin nanosheet-assembled [Ni 3 (OH) 2 (PTA) 2 (H 2 O) 4]· 2H 2 O hierarchical flowers for high-performance electrocatalysis of glucose oxidation reactions. *Nanoscale,* 10**,** 13270-13276.

ZHU, H., LI, L., ZHOU, W., SHAO, Z. & CHEN, X. 2016. Advances in non-enzymatic glucose sensors based on metal oxides. *Journal of Materials Chemistry B,* 4**,** 7333-7349.

ZHU, J., YIN, H., GONG, J., AL-FURJAN, M. & NIE, Q. 2018. In situ growth of Ni/NiO on N-doped carbon spheres with excellent electrocatalytic performance for non-enzymatic glucose detection. *Journal of Alloys and Compounds,* 748**,** 145-153.

ZHU, Y., MENG, X., CHEN, Y., LI, J., SHAO, H., LU, Y., PAN, L., XU, Y. & CHENG, J. 2020. Self-served and fully automated biochemical detection of finger-prick blood at home using a portable microfluidic analyzer. *Sensors and Actuators B: Chemical,* 303**,** 127235.

ZHUANG, Z., SU, X., YUAN, H., SUN, Q., XIAO, D. & CHOI, M. M. 2008. An improved sensitivity non-enzymatic glucose sensor based on a CuO nanowire modified Cu electrode. *Analyst,* 133**,** 126-132.

Internet references

Pine Research. 2019. *Three-Electrode Setups.* https://pineresearch.com/shop/kb/applications/rde-and-rrde/three-electrode-setups/ [12 October 2020].

Phys Org. *Technique to synthesise monolayer films.* https://phys.org/news/2017-08-technique-monolayer.html [12 October 2020].

Labmate. 2011. *Metrohm Autolab: FREE Electorchemical Opne Day – 5th April.* https://www.labmate-online.com/news/laboratory-products/3/metrohm-uk-ltd/metrohm-autolab-free-electrochemistry-open-day-ndash-5th-april/14737 [12 October 2020].

APPENDIX

Appendix A: Supplementary characterisation data

Additional data recorded during physical characterisation of the developed sensors.

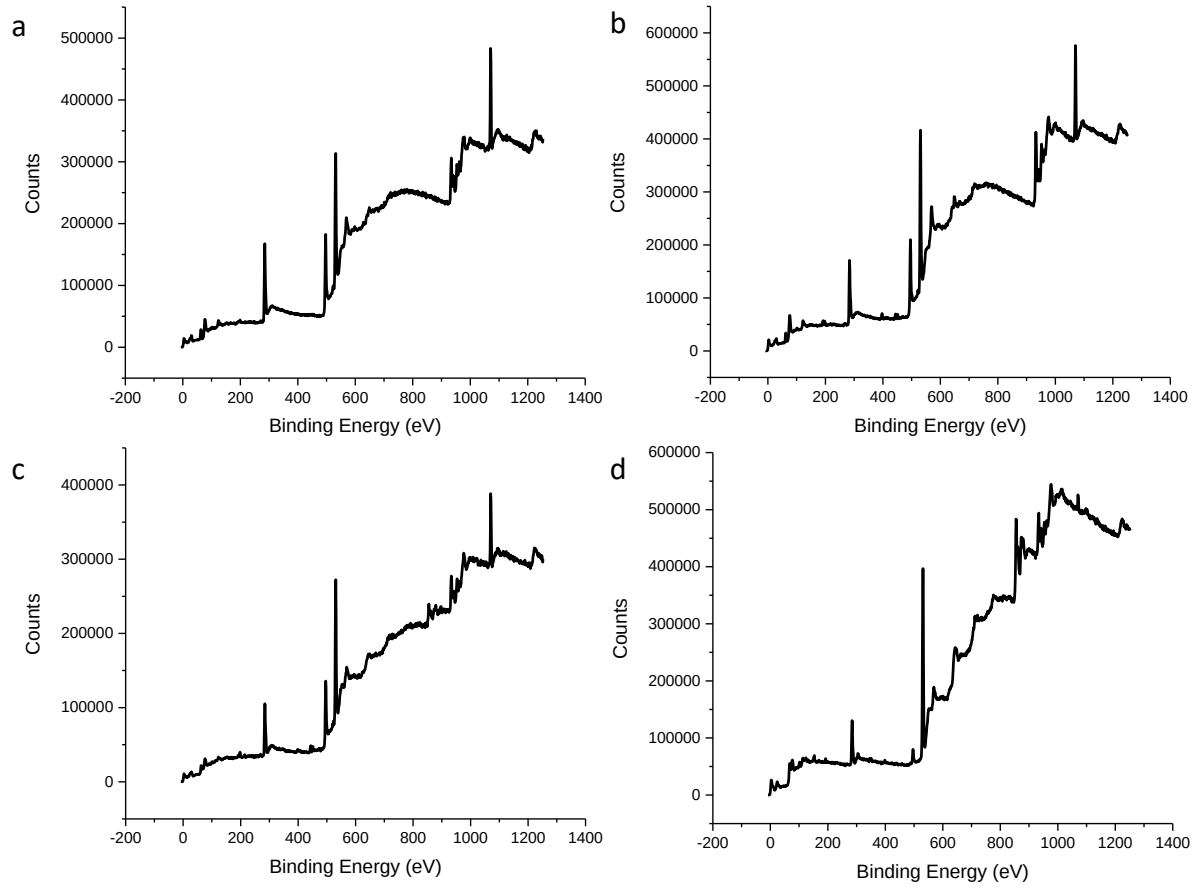

Figure A1 XPS survey scan of a) CuO, b) N-CuO/Cu_2O, c) N-CuO/Cu_2O:NiO and d) N-CuO/Cu_2O:NiO post sensing electrodes

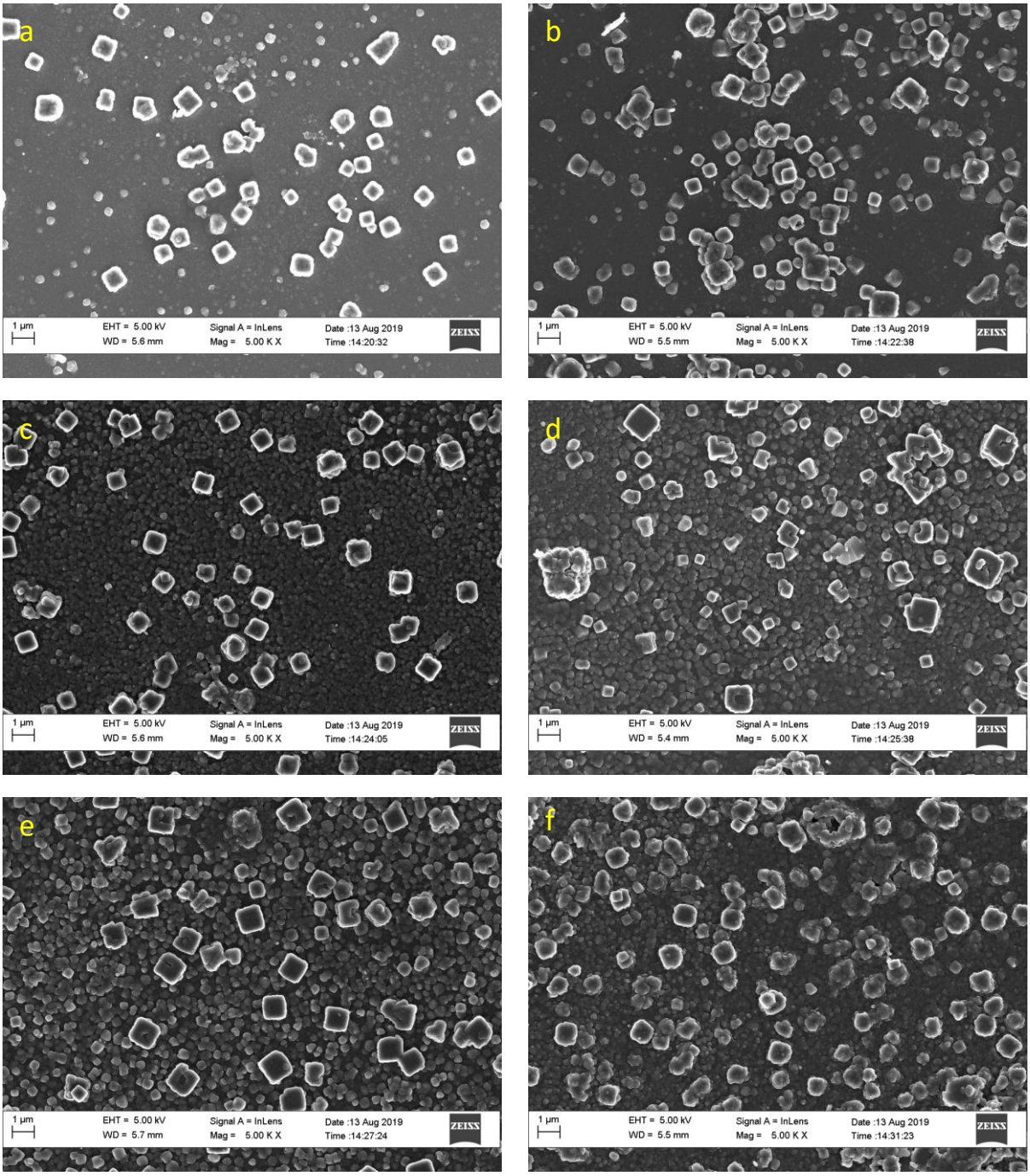

Figure A2 Top view SEM images of N-CuO/Cu_2O:NiO electrode with a) 1 layer, b) 2 layers, c) 3 layers, d) 4 layers, e) 5 layers and f) 6 layers

Appendix B: Supplementary electrochemical results

Results recorded for cyclic voltammograms conducted in 0.1 M NaOH only used to supplement the results recorded under section 4.2.1.

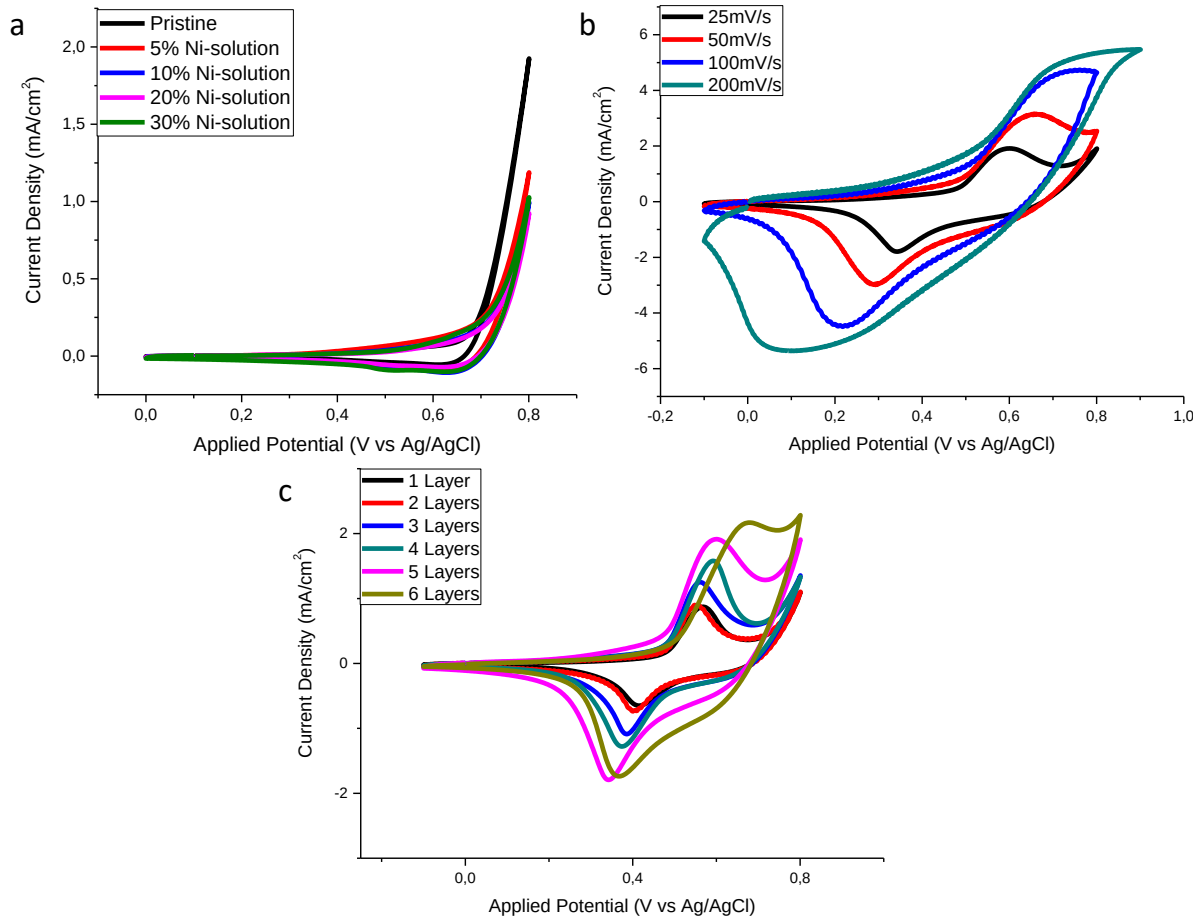

Figure B1 Cyclic voltammograms of a) comparison of the effects of Ni composition on the peak oxidation current, b) various scan rates used for the N-CuO/Cu_2O:NiO electrode and c) layer study of the N-CuO/Cu_2O:NiO electrode

Additional amperometric studies of the CuO, N-CuO/Cu_2O and CuO:NiO electrodes.

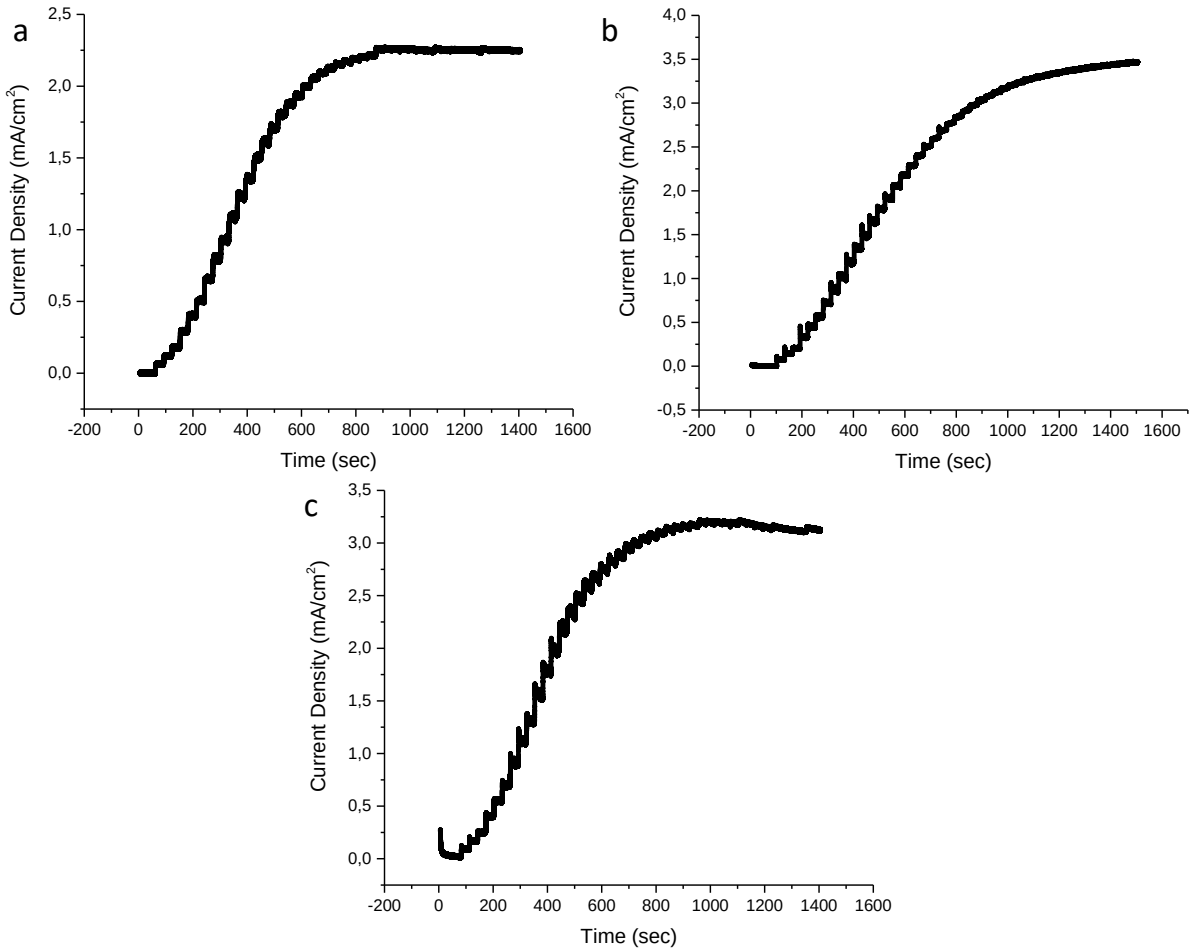

Figure B2 Amperometric response to successive additions of glucose for a) CuO, b) N-CuO/Cu_2O and c) CuO:NiO electrodes

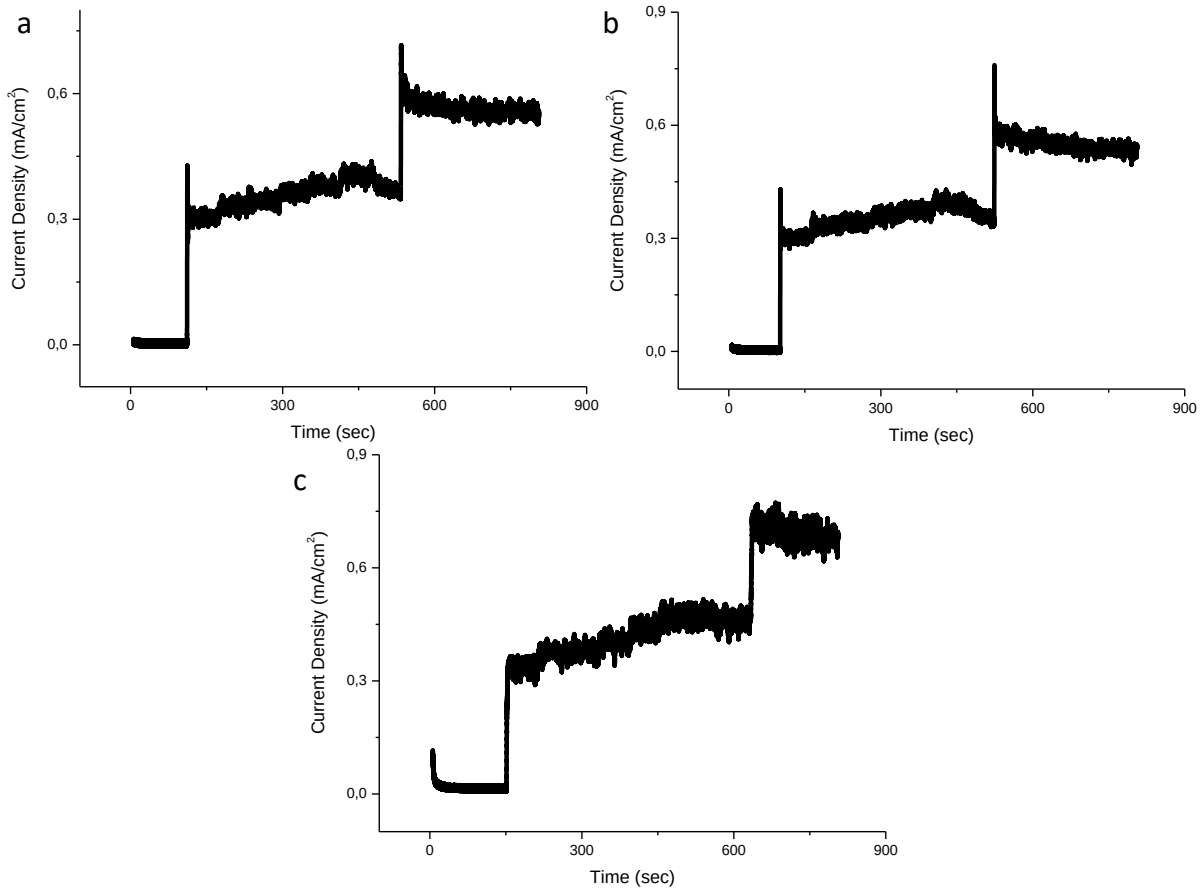

Figure B3 Selectivity test for interference species using a) CuO, b) N-CuO/Cu_2O and c) CuO:NiO electrodes